GEOPHYSICS, VOL. 77, NO. 4 (JULY-AUGUST 2012); P. M53–M72, 19 FIGS., 5 TABLES.
10.1190/GEO2011-0417.1

# Stochastic inversion of facies from seismic data based on sequential simulations and probability perturbation method

Dario Grana[1], Tapan Mukerji[2], Jack Dvorkin[1], and Gary Mavko[1]

## ABSTRACT

We presented a new methodology for seismic reservoir characterization that combined advanced geostatistical methods with traditional geophysical models to provide fine-scale reservoir models of facies and reservoir properties, such as porosity and net-to-gross. The methodology we proposed was a stochastic inversion where we simultaneously obtained earth models of facies, rock properties, and elastic attributes. It is based on an iterative process where we generated a set of models of reservoir properties by using sequential simulations, calculated the corresponding elastic attributes through rock-physics relations, computed synthetic seismograms and, finally, compared these synthetic results with the real seismic amplitudes. The optimization is a stochastic technique, the probability perturbation method, that perturbs the probability distribution of the initial realization and allows obtaining a facies model consistent with all available data through a relatively small number of iterations. The probability perturbation approach uses the Tau model probabillistic method, which provides an analytical representation to combine single probabilistic information into a joint conditional probability. The advantages of probability perturbation method are that it transforms a 3D multiparameter optimization problem into a set of 1D optimization problems and it allowed us to include several probabilistic information through the Tau model. The method was tested on a synthetic case where we generated a set of pseudologs and the corresponding synthetic seismograms. We then applied the method to a real well profile, and finally extended it to a 2D seismic section. The application to the real reservoir study included data from three wells and partially stacked near and far seismic sections, and provided as a main result the set of optimized models of facies, and of the relevant petrophysical properties, to be the initial static reservoir models for fluid flow reservoir simulations.

## INTRODUCTION

One of the aims of reservoir modeling is to describe the spatial variability of reservoir properties: facies and the corresponding petrophysical properties, such as porosity, permeability, net-to-gross, and fluid saturation. The estimation of reservoir properties from seismic data is a complex underdetermined nonlinear inverse problem. Several techniques, both deterministic and probabilistic, have been developed to solve the problem and estimate the optimal reservoir model (Bosch et al., 2010) to be used as initial model in fluid flow simulations. We can classify all the existing methodologies in two categories: (1) multistep inversion methods and (2) stochastic inversion approaches.

In multistep inversion methods, the problem of estimating reservoir properties from seismic data is split into two or more subproblems; generally, elastic properties are first derived from partial stacked seismic data by elastic inversion; then, facies are pointwise classified from the resulting volumes of elastic attributes by statistical techniques, such as, for example, discriminant analysis, neural networks, or Bayesian classification (see Avseth et al., 2001; Mukerji et al., 2001). If a Bayesian elastic inversion (Buland and Omre, 2003) is performed, we obtain in the first step a set of volumes of probability of elastic properties that can be used with a suitable likelihood function to classify seismic facies through the Bayesian approach (Doyen, 2007). In more recent approaches, reservoir properties such as porosity and clay content are estimated from inverted seismic velocities (Grana et al., 2009), and facies distribution can be subsequently derived from the reservoir properties volume. Similarly, in Grana and Della Rossa (2010), a three-step probabilistic approach based on Gaussian mixture models is

Manuscript received by the Editor 19 October 2011; revised manuscript received 13 February 2012; published online 18 June 2012.
[1]Stanford University, Department of Geophysics, Stanford, California, USA. E-mail: dgrana@stanford.edu; dvorkin@stanford.edu; mavko@stanford.edu.
[2]Stanford University, Department of Energy Resources Engineering, Stanford, California, USA. E-mail: mukerji@stanford.edu.

introduced to estimate the probability of seismic elastic attributes, reservoir properties, and lithofluid classes or facies. The traditional Bayesian framework (Tarantola, 2005) also has been adopted for problems of lithofluid prediction from seismic data, as presented in Buland et al. (2008). The probabilistic approach allows us to correctly propagate the uncertainty associated with input data and physical model approximations to the posterior probability of reservoir properties. For non-Gaussian posterior distributions, different estimators can be used to obtain the most likely model, such as mean, median, or maximum a posteriori. However, if the inversion does not include any sampling method of the posterior distribution, the resolution of the estimated properties is the same as that of the input conditioning data (seismic amplitudes) and the final volumes of facies and reservoir properties are representative of a coarser scale than the characteristic scale of reservoir dynamic models. As a consequence, these methodologies require the integration with geostatistical methods to include seismic inversion results into reservoir models (e.g., Mukerji et al., 2001). The most common strategy (Doyen, 2007) is to perform sequential simulations to generate high-resolution facies models by conditioning the simulation with the "coarse-scaled" volume of facies estimated from seismic. Facies models can be generated by two-point (sequential indicator simulation [SISim], e.g., Journel and Gomez-Hernandez, 1989; Deutsch and Journel, 1992) or multipoint geostatistics (single normal equation simulation, e.g., Remy et al., 2009). Both methods allow one to include secondary information derived from seismic data to condition the simulations. The corresponding models of continuous reservoir properties are generated by sequential Gaussian simulation (SGSim), conditioned by the facies model. Other methods recently have been proposed, mainly in reservoir history matching, including geomechanical models to condition reservoir simulations (Wilschut et al., 2011).

On the other hand, stochastic inversion approaches are generally based on the iterative application of a forward model and the inversion step is performed using deterministic or stochastic optimization techniques. In particular, models of subsurface properties (facies and rock properties) are generated; then, suitable rock-physics transforms are applied to generate the corresponding volumes of the elastic properties. Finally, synthetic seismic volumes are computed and compared to real seismic data to evaluate the mismatch. The initial models usually are generated using previously mentioned geostatistical techniques (sequential indicator simulation or multipoint geostatistics, and sequential Gaussian simulation) to create fine-scaled reservoir models (Gonzalez et al., 2008). The final model is found by applying a suitable optimization method. The main limitation of stochastic inversion techniques is that the optimization step in real applications can be computationally expensive. The optimization cannot be applied independently point-by-point because the objective function depends on seismic data that represent coarse scale information reflecting contrasts between subsurfaces. Moreover, as the solution of the inverse problem could have local mimima, the final model could depend on the initial model. Different initial models could lead to different optimized models with the same seismic response, especially when layers thinner than the seismic resolution are included in the reservoir model. Different optimization methods can be used. In Gonzalez et al. (2008), the optimization is deterministic and is performed trace-by-trace. The optimized profile at the current trace then is used to condition the following simulations. Other methods have been introduced: for example, Bosch et al. (2009) propose an iterative optimization based on Newton's method to simultaneously update the multiproperty model. Another family of stochastic inversion approaches is based on Markov chain Monte Carlo methods (Eidsvik et al., 2004; Larsen et al., 2006; Gunning and Glinsky, 2007; Rimstad and Omre, 2010; Ulvmoen and Omre, 2010; Hansen et al., 2012).

We propose a new approach that aims at estimating fine-scaled reservoir models in a stochastic inversion by combining geostatistical methods, such as sequential simulations (Deutsch and Journel, 1992) and a stochastic optimization technique called "probability perturbation method" (PPM), (Caers and Hoffman, 2006), with classical geophysical methods, such as seismic convolution and rock-physics models (Mavko et al., 2009). Our methodology mainly is aimed to determine the optimal facies model for the reservoir. In our approach, we use SISim to generate facies models, and the probability perturbation method to perturb the probability used in SISim. At each optimization step, a new facies model is generated; reservoir properties, in particular porosity and clay content (or net-to-gross), are then simulated by sequential Gaussian simulation conditioned by the facies distribution; elastic properties are subsequently calculated by applying a rock-physics model and converted in the corresponding time domain; and finally, the synthetic seismic response is computed with a traditional convolutional model (Figure 1). The optimization objective function is the two-norm of the difference between the synthetic seismic and the real seismic data. A similar approach has been presented in Gonzalez et al. (2008), with the target being the direct inversion of facies with the integration of rock-physics models and multipoint geostatistics. However, in their

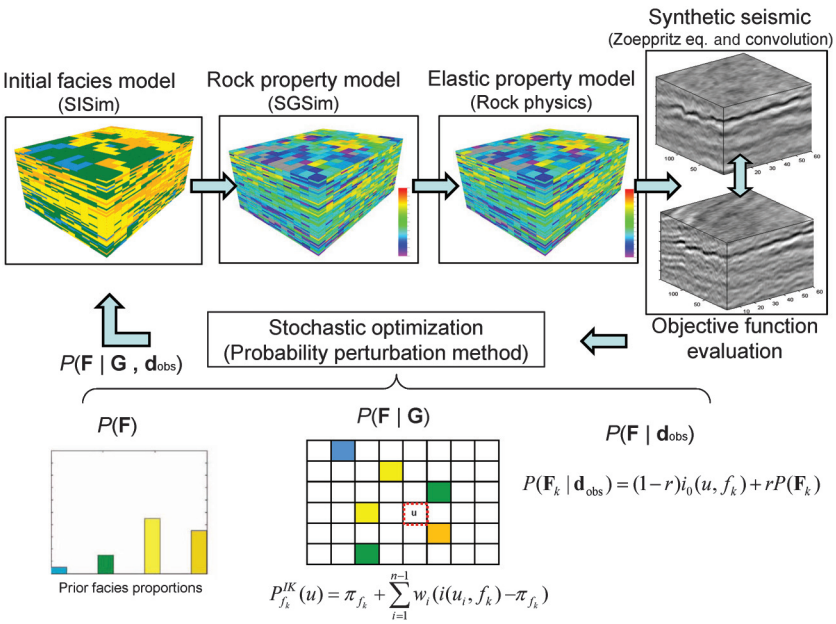


Figure 1. Workflow of stochastic inversion.

method, at each iteration of the optimization, the perturbation of the facies model is performed directly on the realization, whereas in our approach, we perturb the underlying probability distribution used to generate the model. We introduce the probability perturbation method to obtain the optimal model in a reasonable number of iterations. In our methodology, we also account for nonstationarity by introducing an additional probability distribution that can be derived from different sources (seismic or AVO attributes, for example).

We first apply the stochastic inversion to a synthetic case with the objective of reconstructing the actual facies classification, to test the validity of the method. As the proposed methodology includes different methods and models and several parameters have to be calibrated or assumed from prior knowledge or information from nearby fields, we propose a sensitivity analysis that investigates their effect on the corresponding estimations.

The method is then applied to a well log profile and to a 2D seismic section of a real seismic reservoir characterization study in the North Sea (offshore Norway). Several studies have been published on a number of nearby fields in the North Sea (Avseth et al., 2001; Mukerji et al., 2001; Avseth et al., 2005). In this example, we integrated into the methodology a further probability derived from seismic data by means of a traditional Bayesian approach to speed up the convergence and account for nonstationarity.

## METHODOLOGY

The inversion methodology we propose attempts to directly integrate the petroelastic model and facies classification into the seismic inversion workflow. The flowchart of the method is shown in Figure 1. In the following subsections, we will describe each step of the method and the techniques that are used. To clarify the notation, we summarized the symbols in Table 1. The methodology is presented for a clastic reservoir, but it can be adapted to different lithology reservoir conditions with the choice of a reliable rock-physics model and a suitable facies classification.

### Geostatistical methods

The application of geostatistics to reservoir modeling aims to integrate data from various sources (well, seismic, and production data) into a consistent model to describe the rock properties of the reservoir and their spatial continuity.

Sequential simulations are geostatistical methods that can be used to generate realizations of a probability density function of either discrete or continuous properties. These methods are based on various stochastic algorithms and are applied in reservoir modeling to generate different realizations of reservoir properties. This procedure produces high-resolution simulations of the property we are interested in by sequentially visiting the grid cells of a 1D, 2D, or 3D space along a random path. In each cell, the simulated value is drawn from the local conditional distribution, which depends on the prior distribution and on the previously simulated values in the neighborhood of the given cell. This procedure is repeated for all the cells of the grid. The methods available can be divided into two big categories: two-point geostatistics and multipoint geostatistics. Two-point geostatistics algorithms generally are faster as they only account for the correlation between two spatial locations at a time, the spatial continuity of the property distribution being ensured by variogram models. On the other hand, multipoint geostatistics takes into account the correlation between multiple spatial points, but as it is very complex to analytically treat the associated conditional probability, the multipoint statistics are inferred from a training image generated for example by unconditional Boolean modeling. In our approach, we use two-point geostatistics algorithms, but if a suitable training image is available with size at least larger than the reservoir size, then multipoint geostatistics could be easily integrated.

The two most common algorithms in two-point geostatistics are SISim and SGSim (see Deutsch and Journel, 1992; Goovaerts, 1997). Sequential indicator simulation deals with discrete random variables (for example, facies in reservoir modeling), while sequential Gaussian simulation deals with continuous random variables (for example, porosity) (see Appendix A).

In our approach, facies are first simulated by SISim, possibly with a secondary conditioning data derived from seismic (seismic facies probability, for example); then, porosity is simulated by using SGSim. In particular, the simulation of porosity for each facies is performed independently of the simulations for other facies. Each simulation is performed over the whole 3D grid, then the simulations are reassembled into the final simulated porosity realization according to the facies classification. To grid-cells not belonging to the reservoir layer, a constant value of porosity (equal or close to zero) is assigned. Finally, other reservoir properties (for example,

**Table 1. List of symbols.**

| | |
|---|---|
| $\mathbf{F}$ | Facies |
| $f_k$ | $k$th facies value |
| $N_F$ | Number of facies |
| $\mathbf{u} = (x, y, z)$ | Generic spatial location (grid cell) |
| $i(\mathbf{u}, f_k)$ | Indicator variable associated to facies $k$ at location $\mathbf{u}$ |
| $\mathbf{d}_{\text{obs}}$ | Observed seismic data |
| $\mathbf{d}_{\text{synth}}$ | Synthetic seismic data |
| $\mathbf{G}$ | Hard data (facies) |
| $r$ | Deformation parameter |
| $i_r(\mathbf{u}, f_k)$ | Updated indicator variable associated to facies $k$ at location $\mathbf{u}$ |
| $\theta$ | Seismic angle stack |
| $N_\theta$ | Number of seismic angle stacks |
| $\omega_{\theta_k}$ | Weights of the objective function |
| $\mathbf{S}$ | Seismic attributes |
| $\varphi$ | Porosity |
| $ntg$ | Net-to-gross |
| $vclay$ | Clay content |
| $sw$ | Water saturation |
| $\rho$ | Density |
| $K$ | Bulk modulus |
| $\mu$ | Shear modulus |
| $V_{\text{P}}$ | P-wave velocity |
| $V_{\text{S}}$ | S-wave velocity |
| $\mathbf{m}$ | Elastic properties (e.g., $\mathbf{m} = [I_{\text{P}}, I_{\text{S}}]$) |
| $\mathbf{R}$ | Rock properties (e.g., $\mathbf{R} = [\varphi, vclay]$) |

net-to-gross, irreducible water saturation, and also permeability, if necessary) are subsequently simulated by sequential Gaussian cosimulation (CoSGSim) with porosity distribution or previously simulated properties, as secondary information. In CoSGSim, a continuous variable is simulated by accounting for the correlation with another variable; this is the case for example of porosity and net-to-gross or porosity and permeability.

At the end of this step, we obtain a reservoir model of facies, porosity $\varphi$, and net-to-gross $ntg$. In our approach, net-to-gross is transformed into clay content ($vclay$) by assuming $vclay = 1 - ntg$. Fluid saturation distributions (water, oil, and gas saturations, namely, $sw$, $so$, and $sg$) could be simulated as well, but to obtain realistic lithofluid models, we prefer to impose in the model the oil- (or gas-) water contact and the gas-oil contact (if present) and assume a constant distribution of the fluid within the so-obtained fluid layers. To increase the realism of the model, we could, however, simulate the irreducible water saturation through sequential Gaussian simulation or cosimulation or deterministically distribute it by assuming empirical relations with other properties such as porosity or permeability.

One of the favorable features of sequential simulation is the ability to incorporate different types of conditioning data. However, if $A$ is the unknown property and $B$ and $C$ are the conditioning data (for example, hard data $B$ and soft data $C$), then, in many cases, the analytical expression of the posterior probability $P(A|B,C)$ can be difficult to obtain. Journel (2002) has proposed an efficient method to integrate secondary data (soft data $C$) in the probability model $P(A|B)$ to get the posterior probability $P(A|B,C)$. To combine $P(A|B)$ and $P(A|C)$ into $P(A|B,C)$, Journel (2002) proposes the following expression:

$$P(A|B,C) = \frac{1}{1+x}, \tag{1}$$

where

$$\frac{x}{a} = \left(\frac{b}{a}\right)^{\tau_1}\left(\frac{c}{a}\right)^{\tau_2} \tag{2}$$

and

$$a = \frac{1-P(A)}{P(A)}, \quad b = \frac{1-P(A|B)}{P(A|B)}, \quad c = \frac{1-P(A|C)}{P(A|C)}. \tag{3}$$

$P(A)$ is the prior distribution of the unknown property. The ratios $a$, $b$, and $c$ can be interpreted as the distance to an event occurring. For example, the ratio $a$ is the distance to the event $A$ occurring prior to knowing the information associated with $B$ and $C$; if $P(A) = 1$, then $a = 0$ and $A$ is certain to occur. The parameters $\tau_1$ and $\tau_2$ account for the redundancy for each set of conditioning data $B$ and $C$ (Krishnan, 2008). Setting $\tau_1 = \tau_2 = 1$ is equivalent to assuming a form of conditional independence between $P(B|A)$ and $P(C|A)$ expressed in terms of permanence of ratio (equation 2). In other words, we assume that the incremental contribution of data event $C$ to knowledge of $A$ is the same after or before knowing $B$; this assumption is, however, less restrictive than assuming independence between data $B$ and $C$.

The parameter $\tau_2$ can be modified to tune the contribution of the conditioning data $C$; if $\tau_2 > 1$, then the influence of $C$ is increased (in our context, this could be the case where $C$ is crosswell seismic where the resolution is higher than common surface seismic); if $0 < \tau_2 < 1$, then the influence of $C$ is decreased (this could be the case where the quality of the seismic is not optimal and the low resolution of seismic could obscure facies transitions). In our work, we assume $\tau_1 = \tau_2 = 1$, but a preliminary sensitivity analysis at the well location is necessary to investigate the effect of these parameters. Several possible definitions are proposed for the information content measure related to Tau-parameters (Liu, 2003), but the determination of the optimal parameter values is still object of research.

Tau-model formulation allows avoiding the computation of the probabilities $P(B|C)$ and $P(C|A,B)$ or $P(B|A,C)$ that appear in the exact decomposition of $P(A|B,C)$ and that are generally more difficult to calculate. In our application, the unknown property $A$ is the facies classification within the reservoir, $B$ is the hard data, and $C$ is the seismic information.

## Geophysical forward model

To compute the seismic response of the earth models generated by sequential simulations, we first calculate the elastic properties, such as velocities or impedances, within the reservoir model and subsequently compute the corresponding seismic signature. We observe that in many real applications, the geocellular grid (corner-point grid) used to model petrophysical and dynamic properties in the reservoir does not coincide with the seismic grid. In particular, geocellular grid cells usually are larger than the bin size of the seismic survey, which calls for a downscaling of the grid (Castro et al., 2009). Furthermore, the velocity models must be converted from depth domain to time domain to perform seismic convolution and obtain synthetic seismic volumes. Depth-to-time conversion necessarily requires an accurate background velocity model, which is consistent with the seismic processing steps performed on the real seismic data set.

Elastic properties usually are computed through a rock-physics model. This model is a set of equations that transforms petrophysical variables, typically porosity, mineralogy (clay and sand content, for example, in clastic reservoirs), and fluid saturations into elastic properties, such as P-wave and S-wave velocities and density (or, as in many practical applications, P- and S-impedance). The rock-physics model type depends on the reservoir rocks we are dealing with; the set of equations can be a simple regression on well data or a more complex physical model (Mavko et al., 2009). Generally, the model is first calibrated on well logs where petrophysical and elastic properties are available; in fact, most of the models traditionally used contain one or more parameters (for example, critical porosity and coordination number for granular media models, Mavko et al., 2009) that should be determined from core analysis or estimated by comparing well logs and rock-physics model predictions. Once the rock-physics model has been calibrated on well logs, the model is applied, point-by-point, to the volumes of reservoir properties generated by sequential simulations. In the case of a clastic reservoir, these properties are generally porosity $\varphi$, clay content $vclay$, and fluid saturations $sw$, $so$, and $sg$. Clay content is usually computed from net-to-gross as $vclay = 1 - ntg$; this assumption does not account for mineralogical texture related to laminated and dispersed shale that can influence the elastic properties of the rock.

However, if more accurate petrophysical relations linking net-to-gross to lithological properties are available, they can be included in the forward model. The rock-physics forward model can be described as follows: First, we estimate the elastic properties of the solid phase, i.e., bulk and shear modulus of the matrix, $K_{mat}$ and $\mu_{mat}$, and density $\rho_{mat}$ by using solid phase mixing laws (Voigt-Reuss-Hill average or Hashin-Shtrikmann bounds); then, we compute the elastic properties of the fluid phase, i.e., bulk modulus $K_{fl}$ and density $\rho_{fl}$ by using fluid mixing laws (Reuss average or Brie's law); dry rock properties are then computed from solid phase properties by using one of the available theories in literature (for example, granular media or inclusion models) to obtain dry rock bulk and shear moduli $K_{dry}$ and $\mu_{dry}$; finally, the saturated rock properties, $K_{sat}$ and $\mu_{sat}$ are calculated by Gassmann's equations (Mavko et al., 2009). Density of the saturated rock is computed as a linear combination of matrix density $\rho_{mat}$ and fluid density $\rho_{fl}$ weighted by their respective volume fractions

$$\rho = \varphi\rho_{fl} + (1-\varphi)\rho_{mat} \tag{4}$$

and P-wave and S-wave velocities are calculated by definition as function of saturated elastic properties $K_{sat}$ and $\mu_{sat}$ and density $\rho$:

$$V_P = \sqrt{\frac{K_{sat} + 3/4\mu_{sat}}{\rho}}, \tag{5}$$

$$V_S = \sqrt{\frac{\mu_{sat}}{\rho}}. \tag{6}$$

The result of this first step of the forward modeling is a set of volumes of elastic attributes: typically, P-wave and S-wave velocity $V_P$ and $V_S$ and density $\rho$, or P- and S-impedances $I_P$ and $I_S$. The rock-physics model can be facies dependent, such as in the field study we propose in the Application section. Data are subsequently resampled in the seismic grid and converted from depth to time. In our workflow, we downscaled the data using a subsampling technique, but more advanced downscaling methods could be used (Castro et al., 2009). Depth-to-time conversion can be performed by applying a velocity model obtained by collocated cokriging using the stacking velocity volume used for the processing of seismic amplitudes and sonic well-logs filtered at low frequency.

The second phase of the forward modeling step is the computation of the synthetic seismic signature. If partial stacked seismic data ($\mathbf{d}_{obs}(\theta)$) are available, then we compute the corresponding angle stacks. Otherwise, if only post stack data are available, we compute only the zero angle seismic traces. We describe here the partial stack case, as the post stack can be seen as a particular case of this application. Synthetic seismic traces $\mathbf{d}_{synth}(\theta)$ are computed here by seismic convolution; the forward modeling is based on a convolutional model and Zoeppritz equations (Aki and Richards, 1980). Specifically, at each trace, the synthetic seismogram is computed by convolving the wavelets (estimated from the real data set) with the reflection coefficients series:

$$\mathbf{d}_{synth}(t,\theta) = \mathbf{w}(t,\theta) * \mathbf{R}_{pp}(t,\theta) \tag{7}$$

where $t$ is the traveltime, $\mathbf{w}(t,\theta)$ is the vector of the angle-dependent wavelets, and $\mathbf{R}_{pp}(t,\theta)$ is the vector of reflection coefficients. Seismic reflection coefficients $\mathbf{R}_{pp}(t,\theta)$ depend on the angle and the material properties of the subsurface: An isotropic, elastic medium is completely described by P-wave and S-wave velocity and density. For angles smaller than the critical angle of the seismic data set, we can alternatively use a linearized weak contrast approximation of Zoeppritz equations (Aki and Richards, 1980).

We point out that to perform the convolution, we estimate the wavelets independently for each available angle gather. Both forward models, seismic convolution and rock-physics model, lead to underdetermined inverse problems. In our approach, to solve these problems, we adopt a stochastic optimization method in the inversion.

## Stochastic optimization algorithm

The forward model results are included in an optimization loop to find the optimal model of facies ($\mathbf{F}$). We perform a seismic-driven stochastic optimization where the objective function is the two-norm of the difference between synthetic seismic data ($\mathbf{d}_{synth}$) and the real seismic amplitudes ($\mathbf{d}_{obs}$).

The stochastic optimization algorithm we used in our methodology is based on the probability perturbation method (Caers and Hoffman, 2006) and Tau model (see Journel, 2002; Krishnan, 2008). In our approach, the target proportions and the variogram models are assumed to be assigned, but they could be made stochastic and optimized simultaneously. However, preliminary sensitivity tests in 1D showed that the convergence of the algorithm could be more than 10 times slower.

We describe the methodology for a generic reservoir with $N_F$ facies. In particular, the categorical variable $\mathbf{F}$ can assume $N_F$ possible values $f_k$ (for $k = 1, \ldots N_F$). The facies value at a given location is coded using a set of indicator variables $i(\mathbf{u}, f_k)$

$$i(\mathbf{u}, f_k) = \begin{cases} 1 & \text{if } f_k \text{ occurs at } \mathbf{u} \\ 0 & \text{otherwise} \end{cases} \tag{8}$$

where $\mathbf{u} = (x, y, z)$ denotes a generic spatial location corresponding to a grid cell in the reservoir grid.

We first select a random seed and determine a random path of simulation; then, we generate an initial realization of facies by using SISim and according to the selected variogram. We then simulate porosity by using SGSim, cosimulate other rock properties by using CoSGSim and apply the forward model to compute elastic properties and synthetic seismic data. This realization honors the hard data (for example, the facies profiles at the well locations), but it does not necessarily match the seismic data. The initial realization is then perturbed; in the probability perturbation method rather than perturbing the initial realization directly, we propose a perturbation of the probability model used to generate the realization. We denote the underlying probability model of SISim as $P(\mathbf{F}_k|\mathbf{G})$ where $\mathbf{G}$ indicates the hard data (well data or previously simulated values). We remind that in SISim, the probability of facies given hard data $\mathbf{G}$ is obtained at each location by indicator kriging (Appendix A).

At the following step of the optimization, we propose a new probability $P(\mathbf{F}_k|\mathbf{d}_{obs})$ as a linear combination of the indicator model $i_0(\mathbf{u}, f_k)$ associated to the initial realization and the prior probability $P(\mathbf{F}_k)$ of the facies

$$P(\mathbf{F}_k|\mathbf{d}_{obs}) = (1-r)i_0(\mathbf{u}, f_k) + rP(\mathbf{F}_k), \tag{9}$$

where $r$ is the scalar deformation parameter to be optimized between zero and one (Caers and Hoffman, 2006). In our approach, we used a uniform discretization of the interval [0,1] with spacing 0.1, which means that we evaluated the probability in equation 9 for 11 values of the parameter $r$. For each facies, the probability in equation 9 is a function of spatial location $\mathbf{u}$, but for simplicity of notation we omitted the spatial dependency.

At each spatial location $\mathbf{u}$, we now have to combine $P(\mathbf{F}_k|\mathbf{d}_{\text{obs}})$ obtained from equation 9 with the prior probability $P(\mathbf{F}_k)$ and the probability $P(\mathbf{F}_k|\mathbf{G})$ obtained from indicator kriging conditioned to hard data to obtain the probability $P(\mathbf{F}_k|\mathbf{G},\mathbf{d}_{\text{obs}})$. This is done by using the Tau-model (Journel, 2002):

$$P(\mathbf{F}_k|\mathbf{G},\mathbf{d}_{\text{obs}}) = \frac{1}{1+x}, \qquad x = a\left(\frac{b}{a}\right)^{\tau_1}\left(\frac{c}{a}\right)^{\tau_2}, \tag{10}$$

where $\tau_1$ and $\tau_2$ are the Tau-model parameters, and $a$, $b$, and $c$ are obtained by equation 3 with $A = \mathbf{F}_k$, $B = \mathbf{G}$, and $C = \mathbf{d}_{\text{obs}}$. In the case $\tau_1 = \tau_2 = 1$ (i.e, in case of conditional independence), equation 10 simplifies as follows:

$$P(\mathbf{F}_k|\mathbf{G},\mathbf{d}_{\text{obs}}) = \frac{a}{a+bc}. \tag{11}$$

We sample from the distribution $P(\mathbf{F}_k|\mathbf{G},\mathbf{d}_{\text{obs}})$ to generate a new facies model $i_r(\mathbf{u},f_k)$ and we repeat the above-described reservoir modeling by simulating rock properties, computing elastic attributes, and synthetic seismic data $\mathbf{d}_{\text{synth}}(\theta,r)$. For each facies, the probability of equation 10 depends on the scalar parameter $r$; in other words, equation 10 provides a set of distributions and the forward model result is a set of models that depends on the deformation parameter $r$. For each model, we calculate the objective function

$$O(r) = \sum_{k=1}^{N_\theta} \omega_{\theta_k} \left\| \mathbf{d}_{\text{obs}}(\theta_k) - \mathbf{d}_{\text{synth}}(\theta_k, r) \right\|^2, \tag{12}$$

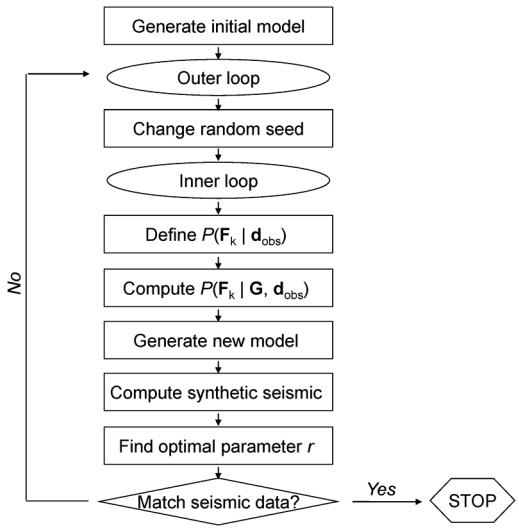


Figure 2. Flowchart of PPM algorithm.

where $N_\theta$ is the number of angle stacks and the $\omega_{\theta_k}$ are the weights assigned to the different angle stacks based on the quality of the seismic data set. For example, we could choose the weights directly proportional to the signal-to-noise ratio (S/N) of the angle stacks. We finally perform a 1D optimization on the deformation parameter $r$.

However, the search space provided by the set of distributions in equation 9 is too limited because it is obtained as a linear deformation of two realizations. Thus, we introduce another optimization loop where we change the random seed and the optimal realization $i_r(\mathbf{u},f_k)$ obtained at the previous step replaces the initial realization $i_0(\mathbf{u},f_k)$.

The optimization step is performed within two nested loops. In the outer loop, we change the random seed until a good match between the synthetic seismic traces of the trial model and the real seismic traces is achieved. At each step, we perform a 1D optimization (inner loop) on the deformation parameter $r$ of the probability perturbation method to obtain the parameter that minimizes the error between the synthetic and real seismic data. If the error of the new model is less than the error of the previous model, we accept the new model and we set $i_0(\mathbf{u},f_k) = i_r(\mathbf{u},f_k)$, otherwise, we change the random seed and repeat the previously described steps. We iterate this procedure until the error is less than a fixed tolerance value $T$, which can be selected depending on the quality of seismic data, for example, in terms of signal-to-noise ratio.

The basic structure of the algorithm (Figure 2) can be described as follows:

1) Select a random seed, generate an initial realization of facies (namely $i_0(\mathbf{u},f_k)$) using SISim, simulate rock properties and apply the geophysical forward model.
2) Perform a seismic-driven stochastic optimization using the probability perturbation method:
   - 2a) In the outer loop, change the random seed and iterate to obtain a good match, i.e., $O(r) < T$.
   - 2b) In the inner loop, perform a 1D optimization to obtain the optimal deformation parameter $r$.

In this inner loop, we propose a new probability $P(\mathbf{F}_k|\mathbf{d}_{\text{obs}})$, obtained as a linear combination of the realization $i_0(\mathbf{u},f_k)$ and the prior probability $P(\mathbf{F}_k)$ of the facies (equation 9). We then compute the conditional probability $P(\mathbf{F}_k|\mathbf{G},\mathbf{d}_{\text{obs}})$ by using Tau-model (equation 10), then generate a new facies model $i_r(\mathbf{u},f_k)$, apply the forward model, and evaluate the objective function of equation 12. If $O(r) < T$, then we stop the algorithm, otherwise, we set $i_0(\mathbf{u},f_k) = i_r(\mathbf{u},f_k)$ and repeat the procedure (steps 2a and 2b), with a different random seed.

## Secondary information

To speed up the convergence, we can include a further probability term in the Tau model, for example, the probability of facies obtained by inverted seismic attributes, $P^*(\mathbf{F}_k|\mathbf{S})$, where $P^*$ represents the pointwise probability of facies conditioned by a set of seismic attributes $\mathbf{S}$ at seismic scale, i.e., at low resolution. The probability of facies at seismic scale can be obtained by using different methods and it can be conditioned by different data, for example, seismic impedances $P^*(\mathbf{F}_k|I_P,I_S)$, seismic amplitudes $P^*(\mathbf{F}_k|\mathbf{d}_{\text{obs}})$, as in Grana and Della Rossa (2010), or AVO properties $R_0$ and $G_r$, $P^*(\mathbf{F}_k|R_0,G_r)$ (see Mukerji et al., 2001). This step allows us to

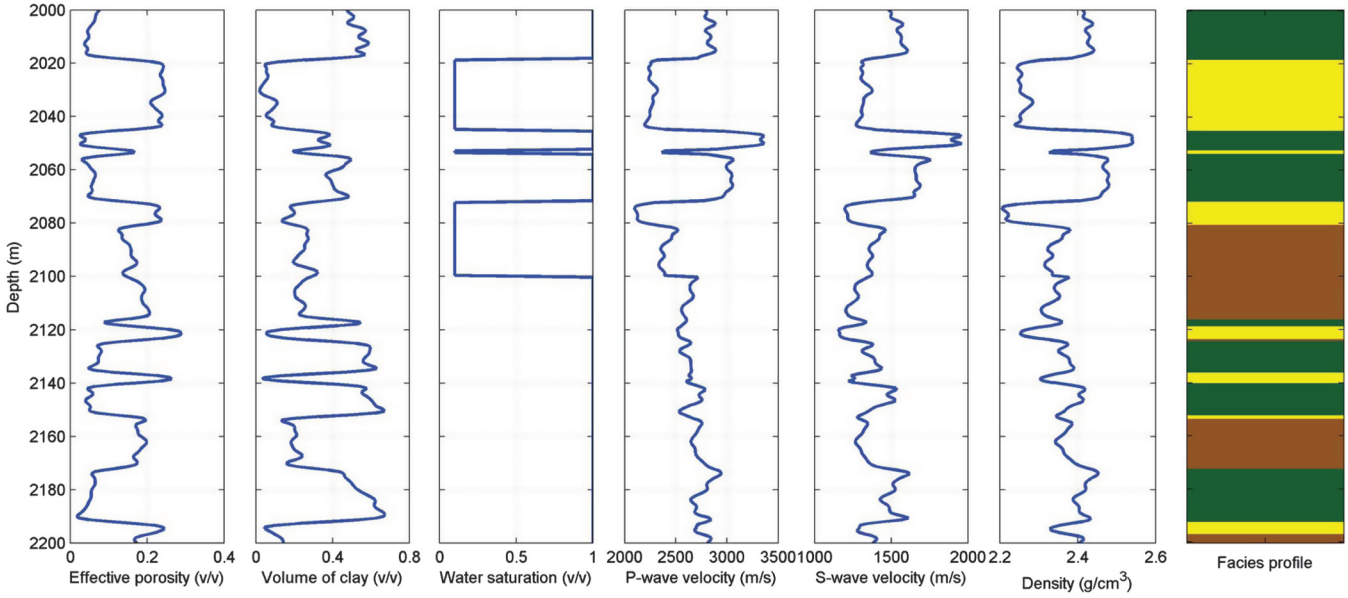


Figure 3. Synthetic well log data set (well A), from left to right: effective porosity, volume of clay, water saturation, P-wave and S-wave velocity, density, and facies profile (green represents shale, brown represents silty-sand, and yellow represents sand).

account for low-resolution secondary information, i.e., the probability of facies conditioned by seismic, which improves the convergence speed and accounts for nonstationarity of the data. The star symbol in the following will indicate the probability of facies at seismic scale used as a low resolution trend to condition stochastic inversion simulations. This probability can be integrated into the workflow in different ways: In our method, we used the Tau-model, by modifying equation 10 as follows:

$$P(\mathbf{F}_k|\mathbf{G},\mathbf{S},\mathbf{d}_{\text{obs}}) = \frac{1}{1+x},$$
$$x = a\left(\frac{b}{a}\right)^{\tau_1}\left(\frac{c}{a}\right)^{\tau_2}\left(\frac{d}{a}\right)^{\tau_3}, \tag{13}$$

where

$$d = \frac{1 - P^*(\mathbf{F}_k|\mathbf{S})}{P^*(\mathbf{F}_k|\mathbf{S})}. \tag{14}$$

However, we point out that other methods could be adopted, such as collocated cokriging or Bayesian updating in sequential indicator simulations (Doyen, 2007).

Different sources of information can be used to obtain low resolution estimation of facies distribution, i.e., to derive the probability of facies at seismic scale $P^*(\mathbf{F}_k|\mathbf{S})$. We adopt a probabilistic approach to seismic facies classification consisting of three main steps: (a) seismic inversion to recover elastic attributes from seismic amplitudes, (b) estimation of petrophysical properties from elastic attributes, and (c) facies classification to classify seismic facies from petrophysical

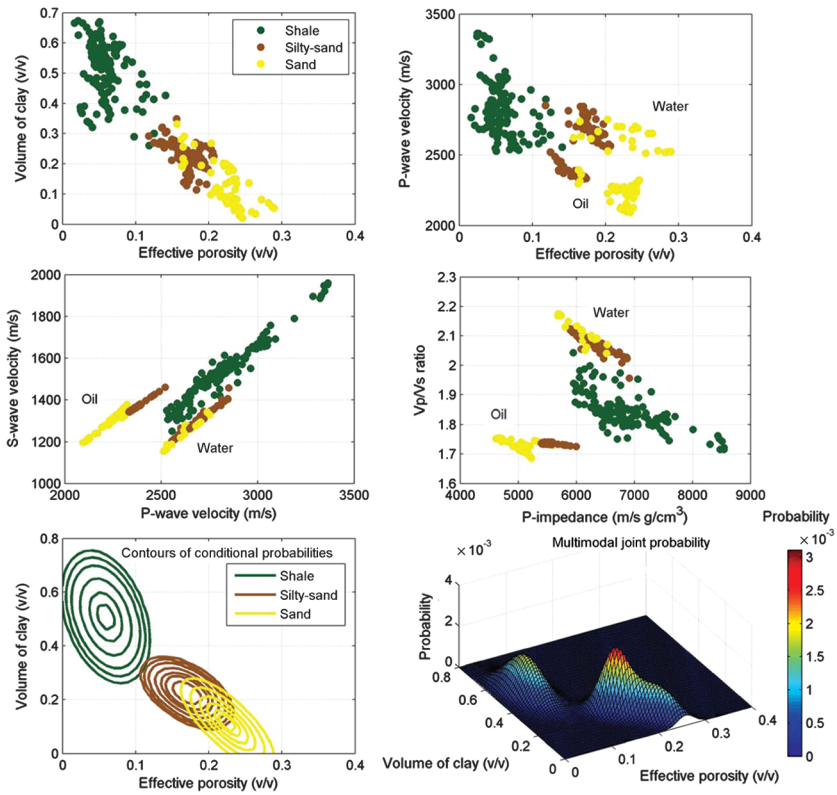


Figure 4. (Top) Rock-physics crossplots of well data set: clay content versus effective porosity (top left), P-wave velocity versus effective porosity (top right), S-wave velocity versus P-wave velocity (mid-left), and $V_P/V_S$ ratio versus P-impedance (mid-right) color coded by facies classification (green represents shale, brown represents silty-sand, and yellow represents sand). (Bottom) Joint probability of petrophysical properties distribution: conditional probability contours color coded by facies (bottom left), and joint probability surface (bottom right).

properties (Grana and Della Rossa, 2010). A full Bayesian approach has been adopted based on the integration of the probabilities obtained from Bayesian seismic inversion and statistical rock-physics model. First of all, a Bayesian seismic inversion is performed (Buland and Omre, 2003) to obtain the probabilities of impedances from seismic amplitudes (step a). Then, a probabilistic characterization of petrophysical properties is applied (Grana and Della Rossa, 2010) to estimate the probability of porosity and clay content (step b) by integrating the statistical rock-physics model with the probabilities of impedances obtained from Bayesian elastic inversion. Finally, a probabilistic facies characterization is performed (Grana and Della Rossa, 2010): The estimation of facies probabilities $P^*(\mathbf{F}_k|\mathbf{S})$ conditioned by seismic attributes (step c) is obtained combining petrophysical properties probabilities (step b), log-facies classification, and seismic information from Bayesian elastic inversion (step a). The mathematical details of this method are presented in Appendix B. The final results of this probabilistic multistep approach are the probability volumes $P^*(\mathbf{F}_k|\mathbf{S})$ of seismic lithofacies that are used in stochastic inversion as additional information in the Tau model to condition the geostatistical simulations and account for nonstationarity.

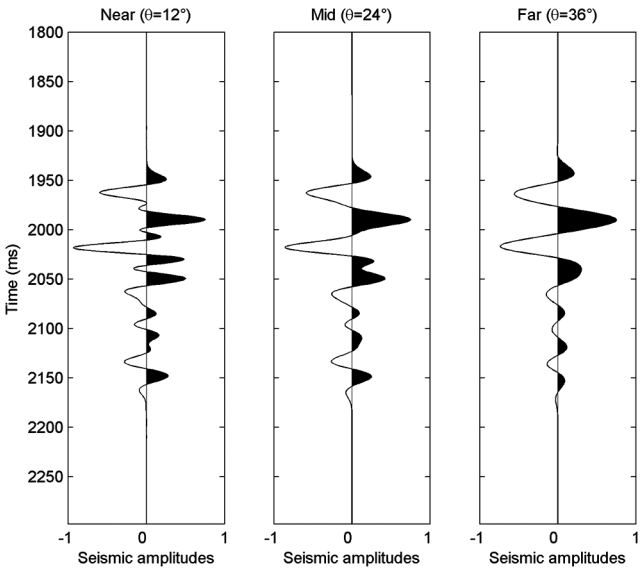


Figure 5. Synthetic partial-stacked seismic data at well location, from left to right: near, mid and far stack, corresponding to the incident angles of 12°, 24°, and 36°.

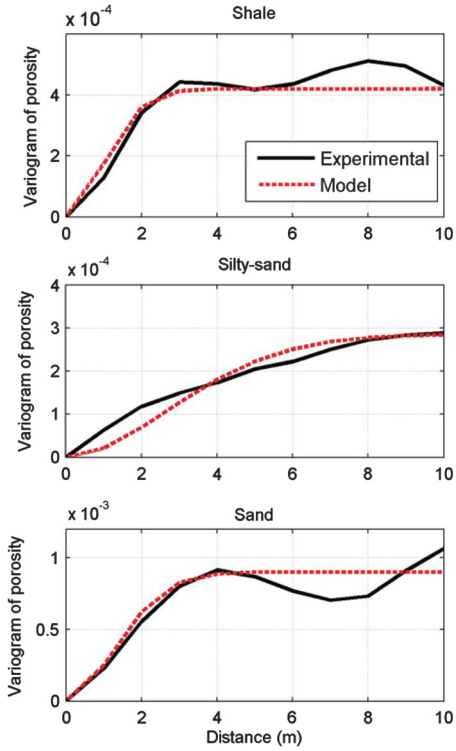


Figure 6. Variograms of porosity estimated at the well location, from top to bottom: variogram of porosity in shale, silty-sand, and sand.

Figure 7. Stochastic inversion results at well location, from left to right: actual facies classification, initial realization, and partial results of the optimization loop after 3, 10, and 25 iterations classification (green represents shale, brown represents silty-sand, and yellow represents sand). The last result (right plot) is the optimized model according to the fixed tolerance.

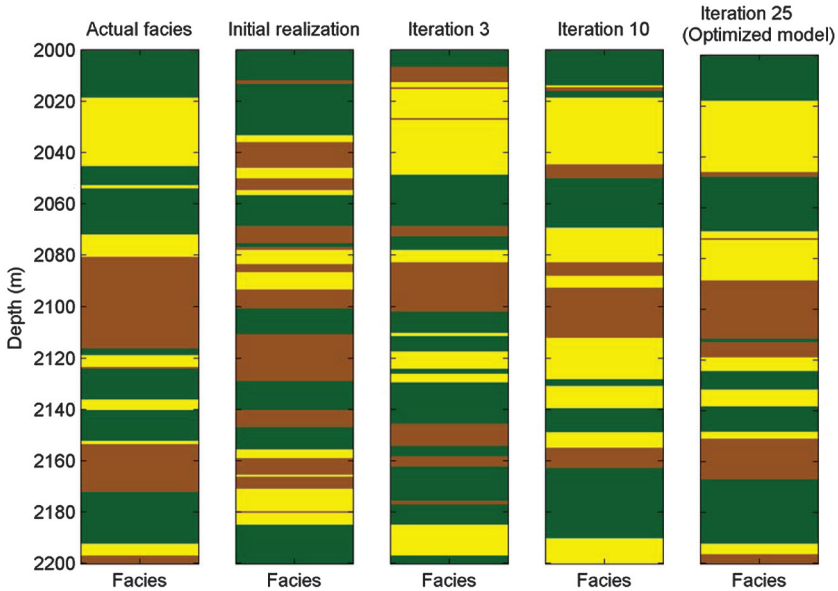

In general, $P^*(\mathbf{F}_k|\mathbf{S})$ can be obtained from any set of seismic attributes, such as inverted impedances, AVO attributes, and full waveform inversion properties; however, the weight of this information, i.e., the exponent $\tau_3$ in the Tau model (equation 13), should be tuned after a sensitivity analysis, as all these properties are derived from the same seismic data set that appears in the optimization objective function. In our application, we tested the following set of parameters $\{0.5, 1, 2.5\}$. By assuming a high exponent $\tau_3$, we increase the convergence speed, but we tend to disregard the prior information related to the spatial continuity model described by the variogram. In particular, we generally obtain a model with a resolution closer to the seismic one. This result can be explained by the fact that we are accounting seismic information in two different terms $c$ and $d$ with a relatively high weight in equation 13. According to the theory, the parameters of the Tau-model measure the additional contribution of the probabilistic information they are associated with. Because the parameter $\tau_3$ is associated with the seismic-derived probability and this information is already accounted for by the probability term $P(\mathbf{F}_k|\mathbf{d}_{\text{obs}})$, we tend to exclude values greater than or equal to one.

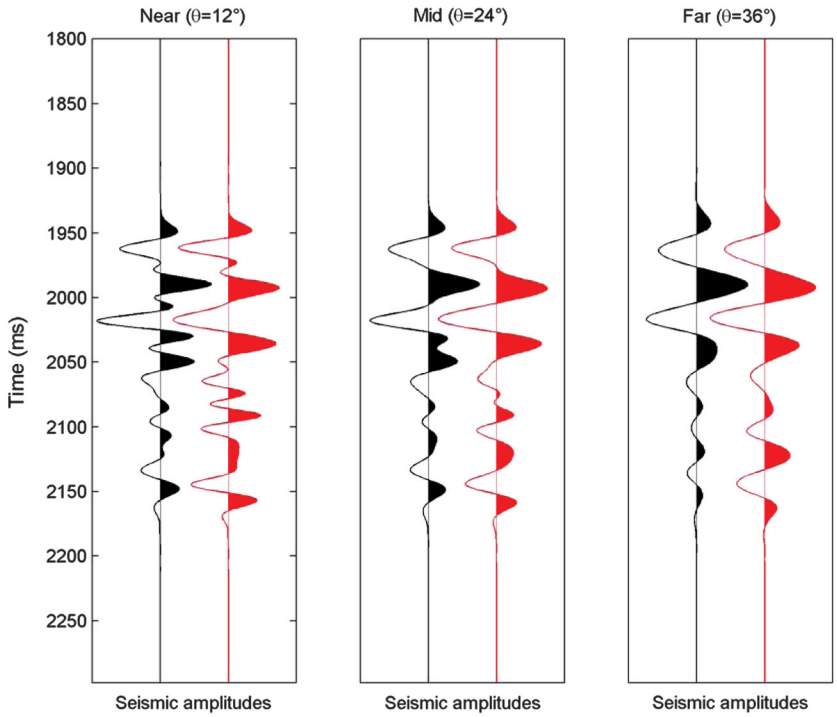


Figure 8. Synthetic seismograms (red) corresponding to the optimized model of Figure 7 compared to input seismic traces (black). From left to right: near, mid and far stack, corresponding to the incident angles of 12°, 24°, and 36°.

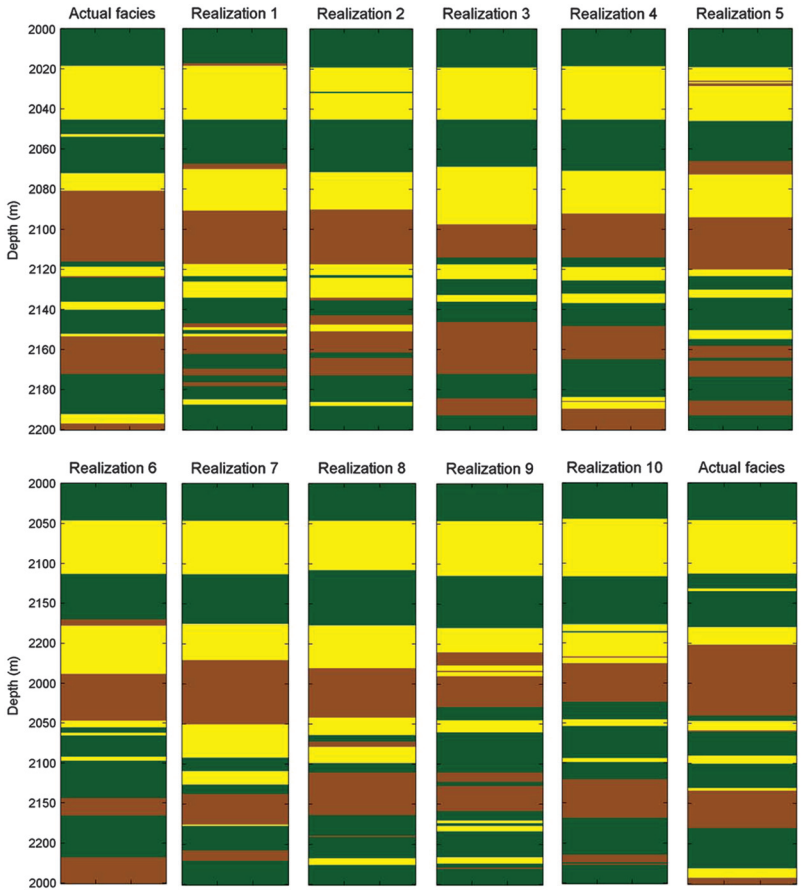


Figure 9. Set of 10 different realizations obtained by stochastic inversion: 10 optimized models (obtained from 10 different runs) compared to the actual classification (green represents shale, brown represents silty-sand, and yellow represents sand).

## APPLICATION

The application of stochastic inversion is first presented in a 1D synthetic case to show the different steps of the method and verify its reliability. Then, we applied the methodology on a real reservoir study in the North Sea where a complete data set, including a set of well log data coming from three wells and partial stacked seismic data, is available.

### Synthetic case

For the synthetic test, we built a set of pseudologs to mimic a realistic depositional turbiditic system along a well profile (namely, well A). This synthetic case models a clastic reservoir filled by oil; the top of the reservoir is supposed to be positioned at around 2000 m depth at the well location and the oil-water contact is fixed at 2100 m. We focus on a depth interval of 200 m, by assuming a thick overcap of clay on top of the reservoir. We created a synthetic facies sequence and a set of pseudologs mimicking the behavior of rock and elastic properties associated to the facies profile, and we finally generated synthetic seismic traces at three different angle stacks: 12°, 24°, and 36°.

**Table 2. Confusion matrix of the reference case (T stands for true facies, C stands for classified facies).**

| | T shale | T silty-sand | T sand |
|---|---|---|---|
| C shale | 0.81 | 0.06 | 0.13 |
| C silty-sand | 0.11 | 0.74 | 0.15 |
| C sand | 0.07 | 0.05 | 0.88 |

**Table 3. One-way sensitivity analysis of the synthetic inversion test: The first column shows the different cases. In the second column, we report the main diagonal of the confusion matrices of the different cases, and in the third column, we show the average of the elements of the main diagonal (sum of the trace of the matrix normalized by the number of facies).**

| | Diagonal confusion matrix | Percentage of identified samples |
|---|---|---|
| True model | 1.00, 1.00, 1.00 | 100% |
| Reference case | **0.81, 0.74, 0.88** | **81.0%** |
| Low signal-to-noise (S/N = 2.5) | 0.76, 0.72, 0.73 | 73.6% |
| Rock-physics model (stiff sand) | 0.92, 0.69, 0.78 | 79.6% |
| Wavelets | 0.79, 0.83, 0.77 | 79.6% |
| Variogram (long range) | 0.71, 0.48, 0.79 | 66.0% |
| Variogram (short range) | 0.76, 0.59, 0.69 | 68.0% |
| Biased prior proportions | 0.93, 0.52, 0.66 | 70.3% |
| Number of angle stacks ($N_\theta = 1$) | 0.55, 0.33, 0.68 | 52.0% |
| Number of angle stacks ($N_\theta = 2$) | 0.84, 0.49, 0.75 | 69.3% |
| Fluid effect | 0.80, 0.76, 0.77 | 77.6% |

Three facies are defined: sand, silty-sand, and shale. We first modeled the synthetic stratigraphic sequence in the well by a first-order Markov chain and then distributed the corresponding rock properties.

Markov chains are a statistical tool that has been used in geophysics to simulate facies sequences to capture the main features of the depositional process (Krumbein and Dacey, 1969). Markov chains are based on a set of conditional probabilities that describe the dependency of the facies value at a given location with the facies values at the locations above (upward chain) or the locations below (downward chain). The chain is said to be first-order if the transition from one facies to another depends only on the immediately preceding facies. The conditional probability of the transitions are the elements of the so-called transition matrix **P**, where the generic element $\mathbf{P}_{ij}$ represents the probability of a transition from the facies $i$ located above the interface to the facies $j$ located below. In our example, we estimated the input parameters, i.e., prior proportions and transition probabilities, from a real well data set. The transition matrix is estimated by counting the number of transitions in the facies classification at the well:

$$\mathbf{P} = \begin{array}{c} \\ sh \\ si \\ sa \end{array} \begin{array}{c} \begin{array}{ccc} sh & si & sa \end{array} \\ \begin{bmatrix} 0.9 & 0.05 & 0.05 \\ 0 & 0.93 & 0.07 \\ 0.05 & 0 & 0.95 \end{bmatrix} \end{array}. \tag{15}$$

Rows correspond to shale, silty-sand, and sand at the generic depth location $z$, and columns correspond to shale, silty-sand, and sand at the generic depth location $z-1$. In other words, in our facies profile, we never have a shale on top of a silty-sand or a silty-sand on top of a sand. The terms on the diagonal of the transition matrix are related to the thickness of the layers; in fact, the higher the numbers are on the diagonal, the higher the probability is that no transition will be observed (i.e., high probability that a facies has a transition to itself), and as a consequence, the thicker the layer will be. We define the first sample of the well profile as shale to have a shale layer above the top of the reservoir. At the next step, the facies value is sampled from the conditional probability $P(F_i|F_{i-1})$, and we iterate the sampling till the bottom of the interval (Figure 3).

Through this method, we generated a facies profile that is assumed to be the true model of this synthetic example. The facies proportions in this well profile are 0.28, 0.34, and 0.38, respectively for sand, silty-sand, and shale. We then generated pseudologs of rock properties, namely porosity and clay content (Figure 3). The pseudologs must be vertically correlated within each facies and at the same time they must be correlated between each other, as porosity in general almost linearly depends on the clay content of the rock. In our data set, we created the pseudologs of porosity and clay content by sampling from three bivariate Gaussian distributions, one for each facies. We assumed a correlation of 0.8 for every facies and we included a vertical correlation by multiplying (Kronecker product) the covariance matrices of each distribution by a spatial covariance matrix obtained from a 1D (vertical) exponential variogram with correlation range 7.5 m (for every facies). The simulated logs finally are reassembled into the final pseudologs according to the facies classification profile. Then, we computed the corresponding pseudologs of density and elastic properties P-wave

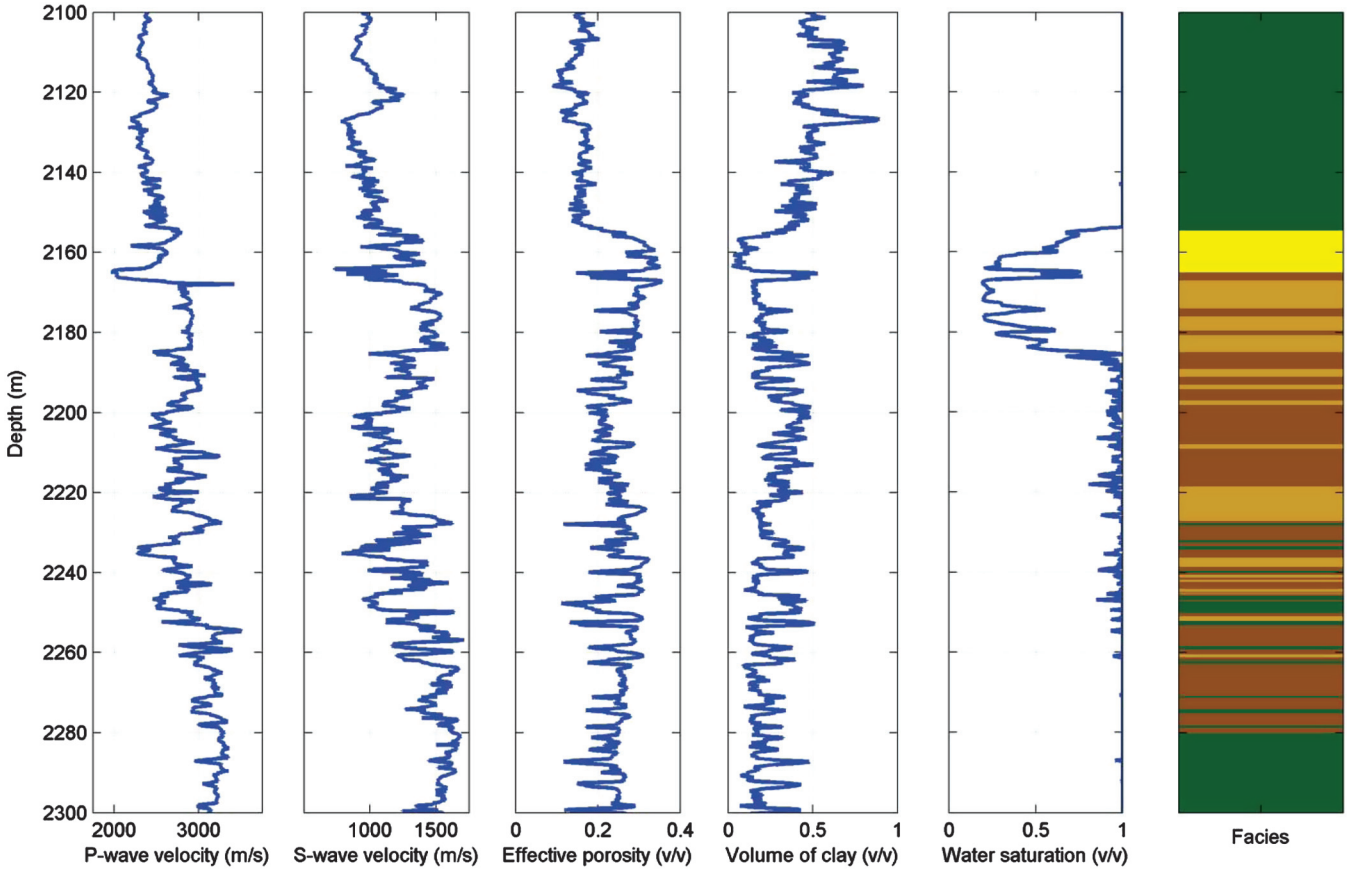


Figure 10. Real case application: well log data set from well two (calibration well). From left to right: P-wave and S-wave velocity, effective porosity, clay content, water saturation, and actual facies classification (shale in green, silty-sand in brown, stiff sand in light brown, soft sand in yellow).

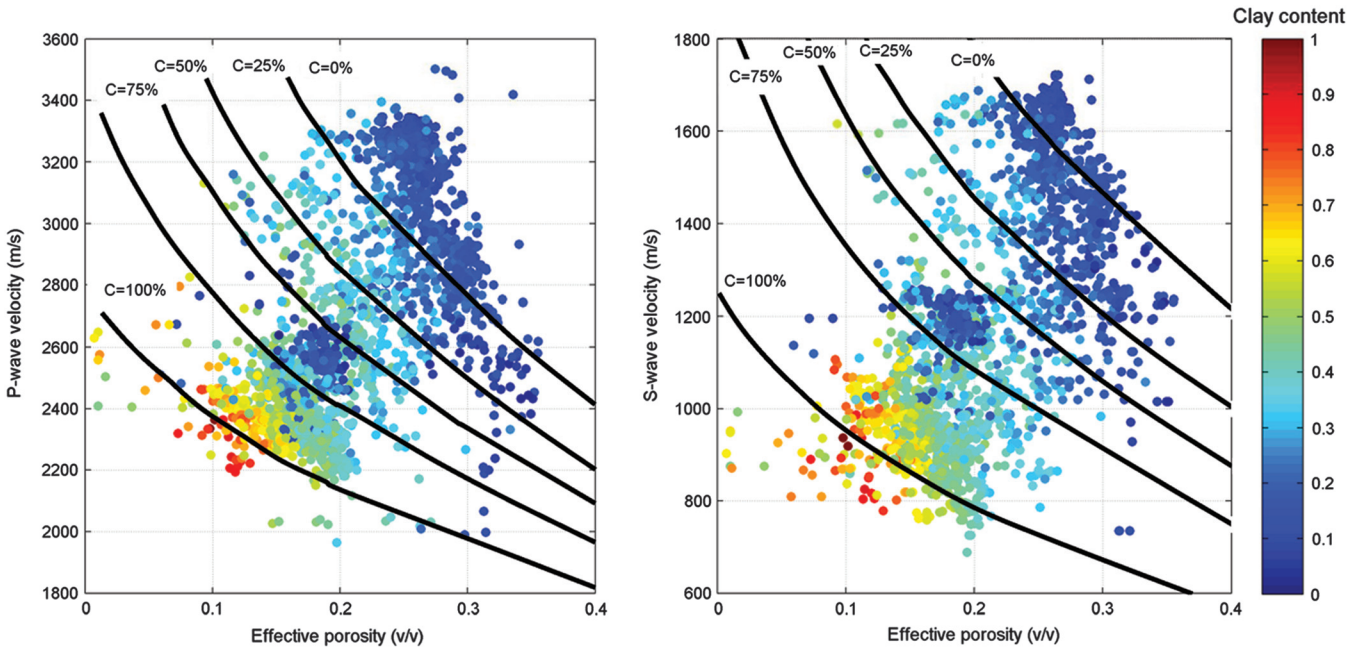


Figure 11. Rock-physics model: (left) P-wave velocity versus effective porosity; (right) S-wave velocity versus effective porosity, color coded by clay content. Black lines represent constant-cement sand model for different clay contents (from top to bottom: 0%, 25%, 50%, 75%, and 100%).

and S-wave velocity by means of the soft sand model (Mavko et al., 2009). Rock-physics models are generally good approximations of the elastic behavior of rocks, but these relations cannot account for the heterogeneity and the natural variability of the rocks in the subsurface. We then added a random error vertically correlated (the correlation range is 1 m) to mimic a more realistic behavior similar to measured well log data. Traditional rock-physics crossplots and

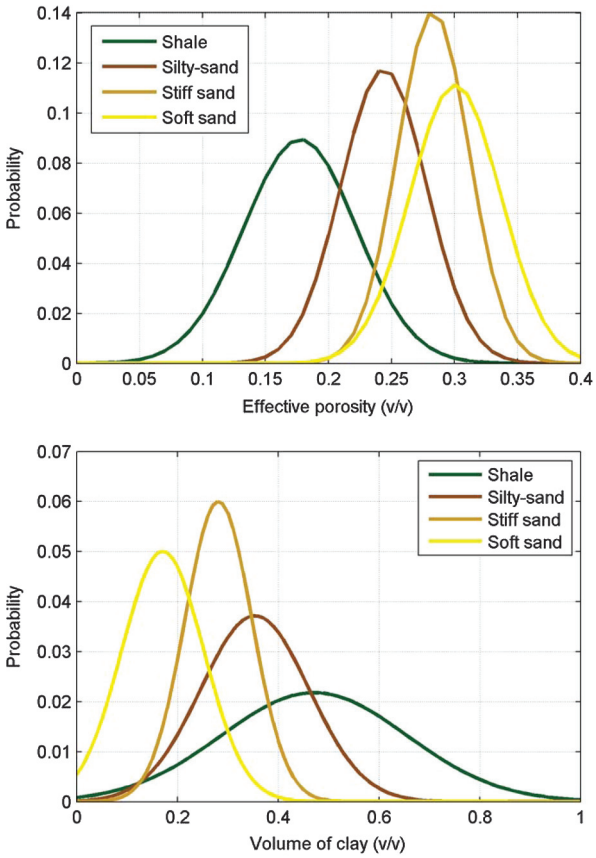


Figure 12. Marginal probability density functions of effective porosity and clay content conditioned by facies classification. The PDFs of petrophysical properties are used to distribute rock properties within the reservoir model at each iteration of stochastic inversion (shale in green, silty-sand in brown, stiff sand in light brown, and soft sand in yellow).

**Table 4. Mean values of petroelastic properties in the different facies. The values of porosity and clay content have been estimated from well log data, and elastic properties values have been computed using the rock-physics model.**

| | Shale | Silty-sand | Stiff sand | Soft sand |
|---|---|---|---|---|
| Porosity | 17% | 24% | 28% | 30% |
| Volume of clay | 47% | 35% | 28% | 14% |
| $V_P$ (m/s) | 2591 | 2872 | 2820 | 2581 |
| $V_S$ (m/s) | 1112 | 1292 | 1313 | 1198 |
| Density (g/cm$^3$) | 2.26 | 2.18 | 2.13 | 2.12 |

the estimated probability distributions are shown in Figure 4. Finally, we computed the synthetic seismograms corresponding to three angle stacks at 12°, 24°, and 36° by using three Ricker wavelets with three different center frequencies at 30, 25, and 20 Hz (Figure 5). PP-reflection coefficients have been computed with Aki-Richards approximation.

In the inversion methodology, we assume that the rock-physics model is known (but the error is unknown) and the three wavelets corresponding to the three angle stacks are known as well. We finally assume that the facies proportions of the true model are known and correspond to the real proportions of the well log profile. The variograms of facies and rock properties used in sequential simulations and the crosscorrelation between rock properties have been estimated from the pseudologs (Figure 6). For the three facies, we assumed a Gaussian model with correlation ranges of 3, 10, and 4, respectively, for shale, silty-sand, and sand.

We show the results of the stochastic inversion methodology applied to the synthetic well A, assuming perfect signal-to-noise ratio in Figures 7 and 8. The facies profile classified by our approach has a good match with the actual classification; good results are obtained after only 25 iterations, which correspond to 275 evaluations of the forward model (because each iteration requires 11 forward model evaluations to locate the optimal parameter $r$). The more we proceed with the iterations, the lower the acceptance rate is. In fact, even if we perform 100 iterations, the improvement compared to the result obtained after 25 steps is quite small. In other words, the stochastic optimization used in this approach quickly reaches a sufficiently small neighborhood of the minimum, then the convergence to the exact minimum becomes slower. We point out that because seismic data generally are noisy, we do not want to match the data perfectly, but only match the data within a certain tolerance ($T$). The convergence can be sped up by introducing secondary information describing the probability of facies at seismic frequency.

We then applied the methodology several times by using different random seeds; the results of the optimization after a fixed number of iterations will be statistically similar, but every time different in the details. In Figure 9, we show the variability between the solutions we obtained by plotting 10 of 25 different runs; this variability mainly depends on the tolerance $T$ we fixed to satisfy the convergence criterion ($O(r) < T$).

Finally, we used this synthetic example to perform a sensitivity analysis on different parameters (for each case, one parameter is changed at a time):

- signal to noise ratio of seismic data: S/N = 5 (good quality seismic) or S/N = 2.5
- rock-physics model: known (we use the same rock-physics model used for the model generation) or unknown
- wavelets: known (we use the same wavelets used for the synthetic seismic generation) or estimated from real seismic data
- variograms: real variogram or a different one with wrong correlation ranges
- prior proportions of facies: real proportions or different ones
- number of angle stacks: poststack seismic or partial stack seismic (two or three angles)
- fluid effect: oil water contact known or ignored

The results of the different cases have been quantitatively compared by computing for each case the corresponding confusion

matrix associated to the facies classification. The confusion matrix is a tool used in supervised learning to visualize the quality of the classification. In our application, each column of the matrix represents the percentage of samples in a predicted facies, whereas each row represents the percentage of samples in the actual facies. The confusion matrix of the reference case shown in Figure 7 (right plot) is summarized in Table 2. For all three facies, we obtain a satisfactory reconstruction rate.

The results of the sensitivity tests are collected in Table 3 where we report the main diagonal of the confusion matrix and the percentage of correctly classified samples (normalized sum of the trace of the confusion matrix). Even though these statistics are not exhaustive to evaluate the quality of the inversion, this sensitivity analysis confirms that the number of angle stacks and the quality of the seismic data are the major sources of uncertainty in seismic reservoir characterization studies. The rock-physics model is essential in this methodology; however, the degree of accuracy of the model is usually quite high because the model can be calibrated at the well locations by using well data. Finally, in our tests, we observed that even if we underestimate the correlation range of the variogram, we still obtain good results in the optimization; conversely, if we overestimate the range, then the optimization model cannot reproduce the correct thickness of the sediments, but it tends to create thicker layers. However, we point out that these results are not completely general and they depend on the parameters we chose. For example, if we use the wrong rock-physics model, but the predictions are close enough to the observed data values (for example, a multilinear regression), or if we ignore the fluid effect, but the velocity in hydrocarbon sand is close to the velocity in brine sand, then the difference between the inversion results with the correct parameters and the ones with wrong assumptions could be small. Similarly, the results of the sensitivity analysis on variogram parameters and prior proportions could be worse if we introduce a more significant bias in the parameters.

## Real case

As a final step, we applied the methodology to a real seismic reservoir characterization study in the North Sea (offshore Norway). It is a deep-water clastic reservoir made of sand and shale and filled by oil. Four seismic-scale sedimentary lithofacies can be identified: soft sand and stiff sand (both filled by oil in the upper part of the reservoir), silty-sand with clay dispersed in it, and shale. The reservoir is located at approximately 2150 m; the oil-water contact was measured at 2190 m at the well locations and it is supposed to be known in the inversion.

The data available are partially stacked seismic data (near stack corresponding to 8° and far stack to 26°), a set of horizons for the reservoir level we are interested in, and five well log data sets. Well two has been used as a calibration well as it contains the main acquired logs: P-wave velocity, S-wave velocity, gamma ray, density, neutron porosity, and resistivity. Data of well two and well three are used to condition the simulations along the 2D line used to test the methodology in 2D. Finally well five, located outside the seismic survey, is used as an additional test.

First, the method has been tested at the well two location to predict the facies distribution from seismic data. The lithofacies classification has been performed using sedimentological information, core analysis, and a clustering technique applied to petrophysical curves: effective porosity, volume of clay, and volume of sand (Figure 10). A rock-physics model has been calibrated at the well location; the more suitable model for this scenario is a constant-cement sand model (Avseth et al., 2005). This model is a combination of the contact-cement model and friable sand model (Mavko et al., 2009), where we assumed a critical porosity equal to 0.4 and a coordination number of nine (Figure 11); however, we point out that in some wells (wells two and five), we can identify a relatively thick layer of soft sand at the top of the reservoir; therefore, in this facies, a soft sand model has been applied to explain the low-velocity values measured at the well locations in the corresponding intervals. From well data, we also can infer the marginal distribution of petrophysical properties conditioned by the facies classification (Figure 12); the estimated PDFs are used in the forward model to generate the simulated realizations at each iteration of the stochastic inversion. We assumed for simplicity, Gaussian distributions, but SGSim does not require that the prior distribution is Gaussian and other distributions could be used. The descriptive statistics of the different properties are shown in Table 4.

The results of the 1D application with a perfect synthetic seismic trace ($S/N = \infty$) are shown in Figure 13, where we reconstruct the lithofacies classification at the well two location. In this test, we assumed that the wavelets were known. In other words, the wavelets used in the inversion were the same as those used in the forward modeling performed to generate the synthetic seismic trace. The actual facies profile is severely nonstationary and the estimation of variogram parameters was not reliable; we then assumed the same exponential model for all the facies with correlation range

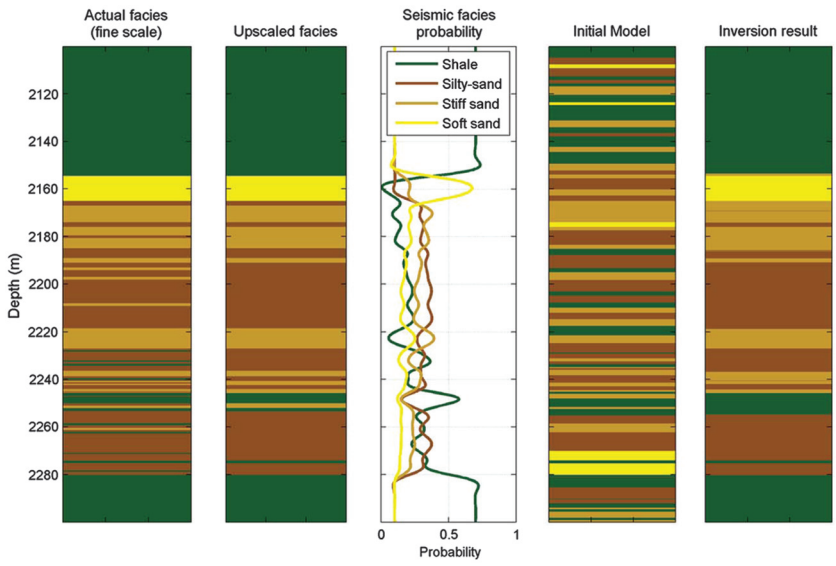


Figure 13. Inversion results at well two location with synthetic seismic data, from left to right: actual facies classification, upscaled facies profile, seismic facies probability, initial model, optimized model after 50 iterations (shale in green, silty-sand in light brown, stiff sand in brown, and soft sand in yellow).

equal to 2.5 m. We notice that even if we start from an initial model with a short vertical correlation range, we obtain a good result in the inversion: After 50 iterations (right plot), the error between the input seismic and the synthetic seismic generated from the optimized model is lower than the fixed-tolerance $T$', and the match between the optimized facies profile and the actual classification is satisfactory. The tolerance $T$' is fixed such that the ratio between the variance of the signal and the variance of the residuals approximates the S/N. In this example with perfect synthetic seismic, we stop the convergence when the ratio approximates 10. The upscaled classification (see Stright et al., 2009) over a support of 1 m is provided for comparison. As already pointed out, the tolerance value used to stop the inversion process depends on a number of factors, in particular, the quality of seismic data (signal-to-noise and resolution). The more reliable is the seismic data set, the smaller the tolerance can be. In most of the cases, we do not want to perfectly match the seismic data, but we aim to obtain a model (or a set of models) that match the data within a fixed tolerance. In Figure 14, we show two different sets of inverted models; on the top, we show 25 inverted models obtained by imposing a small tolerance $T$' (on average, 51 iterations are needed to reach the required accuracy); on the bottom, we show 25 inverted models obtained with a larger tolerance equal to $1.2T$' (33 iterations required on average). By decreasing the tolerance value, we improve the match between the input seismic and the synthetic seismic of the generated models, but we increase the computational time to reach the convergence

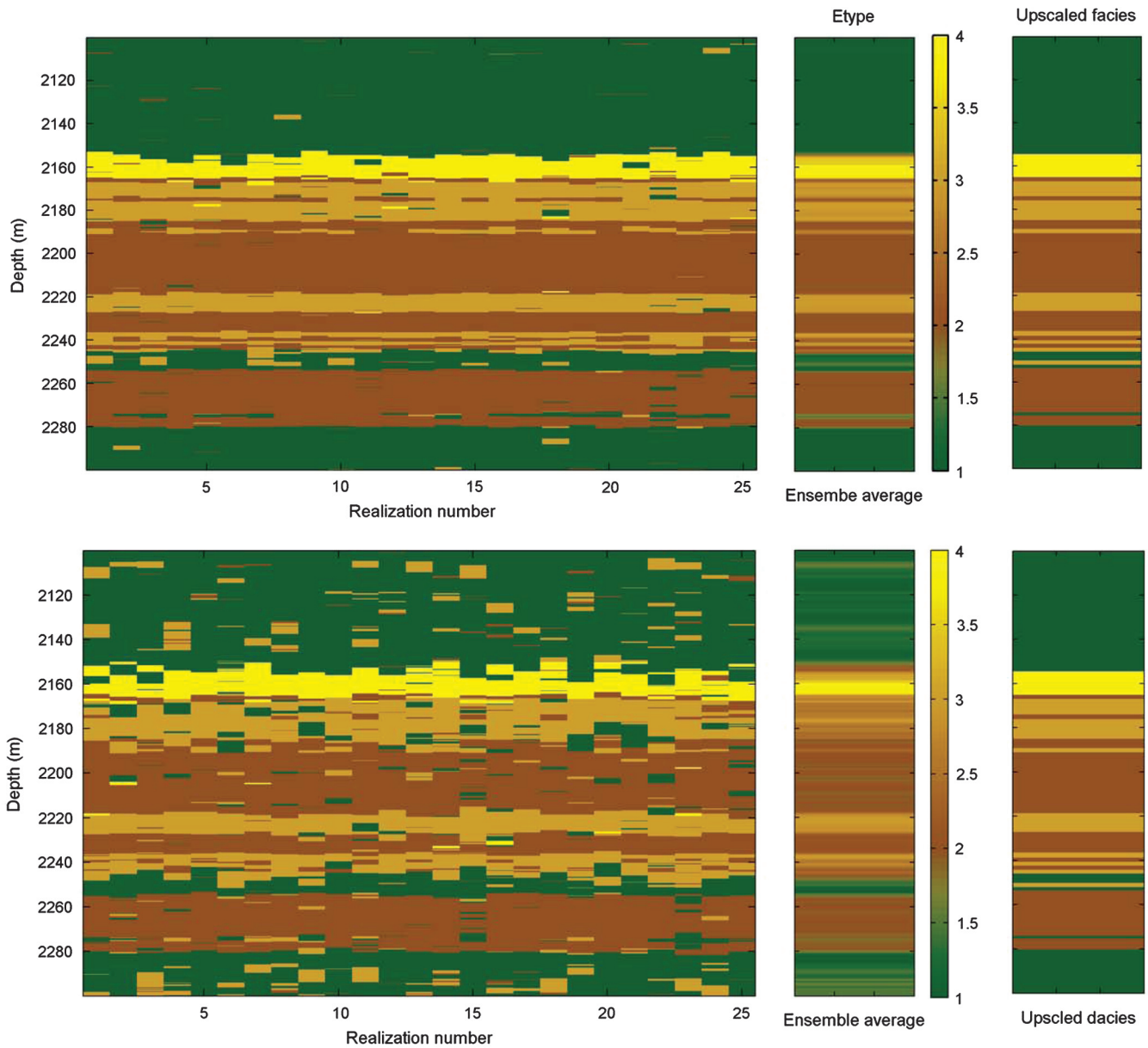


Figure 14. Multiple realizations with different tolerance conditions: (top) 25 simulations obtained with a small tolerance; (bottom) 25 simulations obtained with a larger tolerance (shale in green, silty-sand in brown, stiff sand in light brown, and soft sand in yellow). For each set of simulations, we plot the ensemble average (e-type) and compare the results with the upscaled facies classification at well two location.

condition. The different variability within the two sets of realizations is shown by the e-types of the two ensembles (Figure 14). The e-type is the ensemble average of the set of models and it is a continuous variable.

We then performed the same inversion exercise with the real collocated seismic trace (Figure 15). The quality of the inversion is worse than the previous case, but it is still satisfactory as pointed out by the confusion matrix reported in Table 5, where we obtain high recognition indexes for all the facies. In both applications with synthetic and real seismic, we used a low resolution probability estimated at the well location as secondary information. In this application, we assumed that the parameters of the Tau-model are: $\tau_1 = \tau_2 = 1$ and $\tau_3 = 0.5$. The use of this probability is necessary to account for the nonstationarity of the actual facies classification. In Figure 16, we show the convergence of the methodology with and without secondary information and we show the boxplots of the normalized error of 25 optimization runs, each of them consisting of 50 iterations. We notice that the convergence is much slower if no secondary information is used, and the average error is generally higher.

We then applied the methodology to two other wells (wells three and five) by using the same parameters for variograms, prior distributions of properties, and forward models calibrated at well two. Well three does not present soft sand in the classification, whereas the scenario in well five is similar to the calibration well. In both cases, the inversion results are good (Figure 17), even though we notice that we cannot reproduce the thin layers below a certain thickness. We could actually obtain a set of models with the same vertical correlation observed at the well by using a shorter correlation range and a larger tolerance $T$ and/or a smaller value of the Tau-model parameter $\tau_3$ (equation 13) related to the low-resolution information. In fact, if we assign a high weight to seismic data (low-tolerance $T$ and/or high-parameter $\tau_3$), we tend to match the seismic data with higher accuracy and we cannot recover thin layers under the seismic resolution. If a larger tolerance is fixed or a lower weight is assigned to seismic data, we could recreate thin layers according to the input variograms; however, in this application, we retain that some of the layers visible in the actual profile are due to clustering artifacts in the log-facies classification process.

As conclusion of this study, we perform the stochastic inversion in terms of facies of a 2D seismic section passing through wells two and three. The near and far stacks are shown in Figure 18 and the horizon (in time domain) of the top reservoir is superimposed. The seismically derived probability of facies $P^*(\mathbf{F}|\mathbf{S})$ has been computed following the approach proposed in Grana and Della Rossa (2010) (Appendix B). The maximum a posteriori of the so-estimated seismic facies probability converted in depth within the geocellular grid, is shown, as a reference, in Figure 19 (bottom right). The velocity model used for the time-to-depth conversion has been obtained by applying a kriging method to the 2D section and by using filtered sonic logs (at a frequency of 4 Hz).

The initial model has been generated using SISim. The 2D variograms of the facies have been estimated using information from previous studies on this field and nearby fields of the same area, and the prior information assumed by averaging the facies proportions at the well locations. The 2D variograms describe the spatial continuity model of the facies. For each facies, we assumed an exponential model with the following parameters: The lateral correlation range is 1000 m for soft sand, 2000 m for stiff sand, 2500 m for silty-sand, and 800 m for reservoir shale; the azimuth is 0° for all the facies. The optimization is performed for all traces simultaneously.

The main result of this study is the optimized facies model (Figure 19, top). This result honors the prior information and the spatial continuity of the data; furthermore, the optimized realization honors the seismic data. Here, we show the results after 10 iterations, corresponding to 110 2D simulations, in terms of facies, porosity, P-wave velocity, and the corresponding synthetic seismic (Figure 19). For simplicity, the porosity of the nonreservoir shale has been set constant equal to 0.05. As expected, the areas with higher variability are the sequences of silty-sand and stiff sand in the lower part of the reservoir.

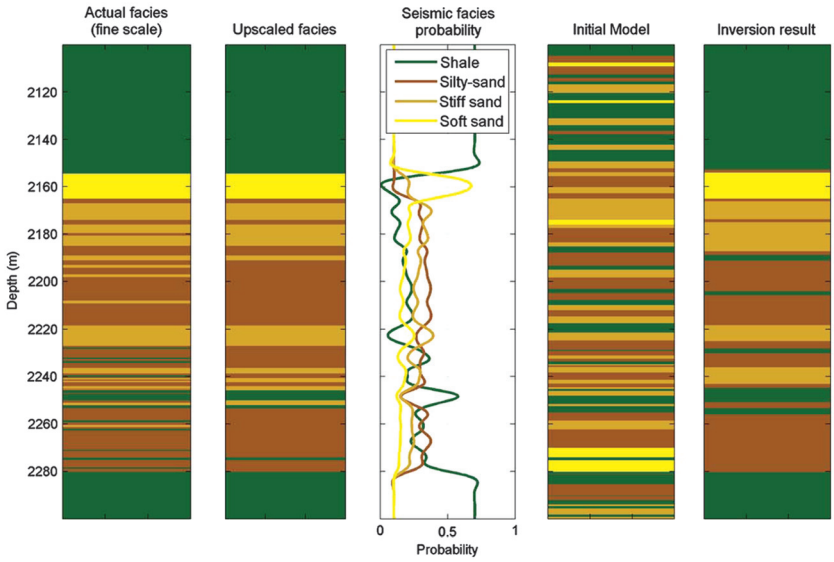


Figure 15. Inversion results at well 2 location with real seismic data, from left to right: actual facies classification, upscaled facies profile, seismic facies probability, initial model, optimized model after 50 iterations (shale in green, silty-sand in brown, stiff sand in light brown, and soft sand in yellow).

**Table 5. Confusion matrix of the inversion results obtained by stochastic inversion at well two location (T stands for true facies, C stands for classified facies).**

| | T shale | T silty-sand | T stiff sand | T soft sand |
|---|---|---|---|---|
| C shale | 0.95 | 0.05 | 0 | 0.00 |
| C silty-sand | 0.09 | 0.81 | 0.10 | 0 |
| C stiff sand | 0.07 | 0.08 | 0.72 | 0.13 |
| C soft sand | 0 | 0.10 | 0 | 0.90 |

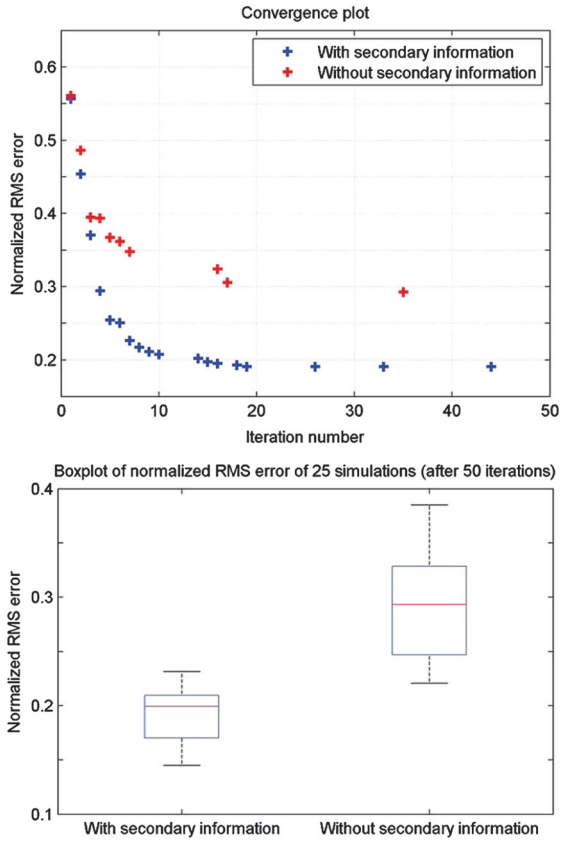


Figure 16. (Top) Convergence plot of stochastic inversion results (single run) with and without low-frequency information (blue and red symbols, respectively) as a function of iteration number. (Bottom) Boxplots of 25 runs consisting of 50 iterations with and without low-frequency information (left and right, respectively).

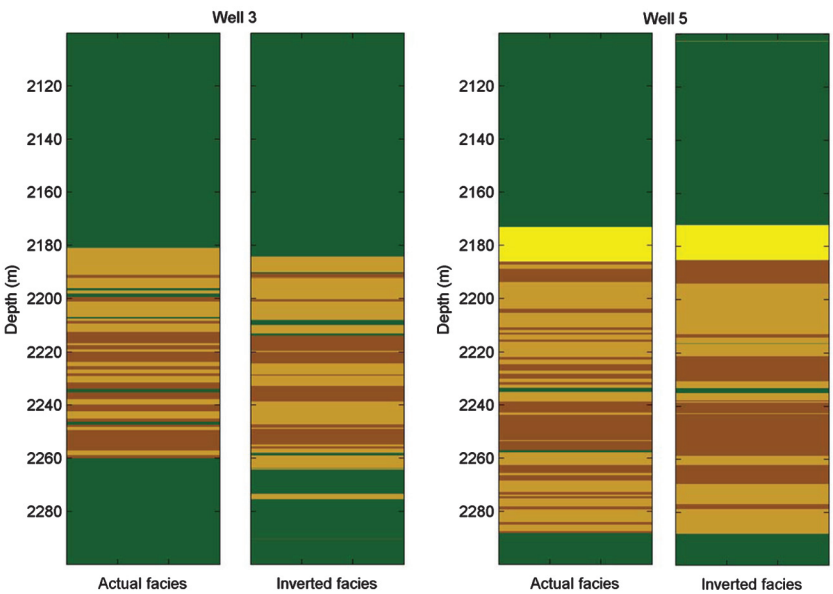


Figure 17. Inversion results at well three (left plots) and well five (right plots) locations. We compare the actual classification with the optimized model obtained by stochastic inversion (shale in green, silty-sand in brown, stiff sand in light brown, and soft sand in yellow).

As this application points out, the main advantage of stochastic techniques is that the estimated facies model has a higher resolution than the model obtained from the maximum a posteriori of the probability of facies directly inferred from seismic, and it can be directly used as initial model in fluid flow simulation, without the integration of additional geostatistical methods.

## DISCUSSION

In this paper, we summarized the main results obtained by applying a new methodology for inversion of seismic data in terms of facies. Most of the geostatistical methodologies published so far require large computational times to be performed for real reservoir studies. The introduction of the probability perturbation method allows us to reduce the computational time, compared to other stochastic optimization methods. The probability perturbation method incorporates the Tau model, which is a probabilistic model to account for information coming from different sources. By using the Tau model, we can integrate well and seismic data and we could potentially extend the methodology to include other information such as EM data or production data.

In our approach, we used two-point geostatistics methods to obtain models of facies and petrophysical properties; however, the presented stochastic inversion could be applied also with multipoint based priors if a suitable training image is available. Multipoint geostatistics could be necessary in lithofluid inversion to avoid nonphysical scenarios such as brine sand on top of oil sand. In our study, we assumed that the oil-water contact was known.

We point out that in both cases, it is important to include secondary information in the methodology, specifically in the Tau model; this information represents the probability of facies at seismic scale, or in a broad sense, the low-resolution probability of facies. This additional step has two goals: The first one is to speed up the convergence as shown in our application, and the second is to account for nonstationarity. Two-point and multipoint geostatistics are based on the assumption of stationarity, but in most of the cases this assumption is not completely satisfied. In our real case application, for example, silty-sand and stiff sand approximately have a stationary behavior in the reservoir layer, but this is not true for soft sand, which appears only at the top of the reservoir. The scenario is more complex if we consider the shale layers at the top and at the bottom of the reservoir. The layers bordering the reservoir can be neglected in reservoir modeling if a reliable set of horizons is provided; however, in seismic reservoir characterization, the elastic contrasts at the top and at the bottom of the reservoir have a key role in seismic interpretation and inversion. The introduction of the probability of seismic facies, even with a low resolution, allows us to account for the nonstationarity observable in the vertical stratigraphy. Moreover, we observed in the proposed real-field application that the integration of the secondary probability information reduces the number of iterations by a factor of five (assuming $\tau_3 = 0.5$). We point out that secondary information could be integrated in different ways. In addition to the Tau model used

in our research, we could include this additional probability data in sequential simulations by using cokriging or Bayesian updating. The secondary information could be derived from different sources of information, such as full waveform inversion, AVO attributes, or EM methods.

Nonstationarity also is visible in petrophysical and elastic properties and it can be recognized by the presence of trends as a function of depth. To overcome this issue, we introduced in the real-case application a deterministic trend of porosity and elastic properties to integrate/correct the rock-physics model which does not explicitly account for depth-dependency. The trend observable in porosity could be due to different mechanisms and also to changes in lithology; for example, we suspect that the layer of shale at the bottom of the reservoir has a different mineralogy than the overcap clay, even though the amount of clay recognized by gamma ray log is approximately the same. In general, the depth trend is not linear (see Rimstad and Omre, 2010) and several models are available, but in a relatively small depth interval, it can be approximated by a linear regression.

We observe that, in the forward modeling, we used a convolutional model, which is a Born

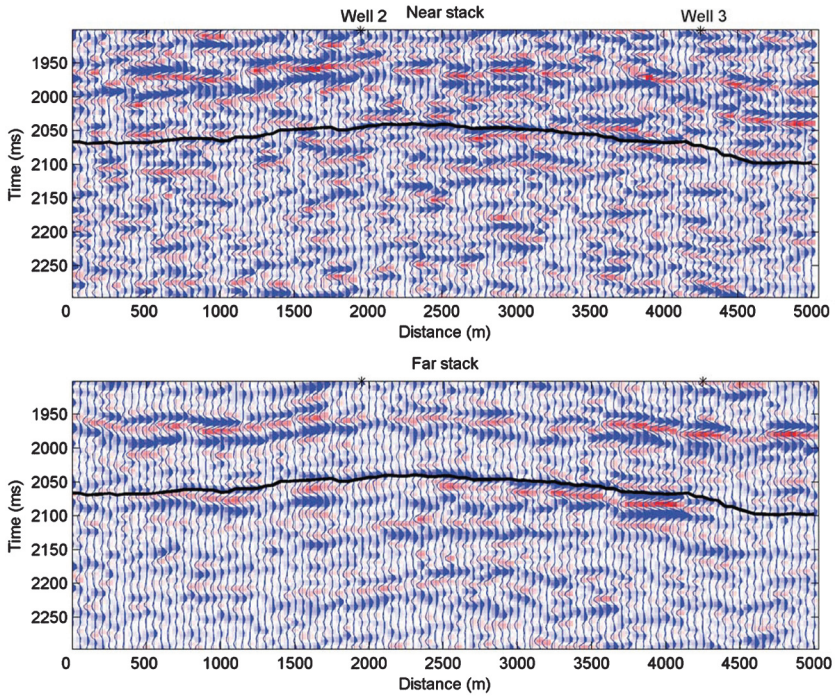


Figure 18. 2D seismic section passing through wells two and three: (top) near angle stack corresponding to 8°; (bottom) far angle stack corresponding to 26°. The black line represents the horizon, in time domain, corresponding to the interpreted top of the reservoir.

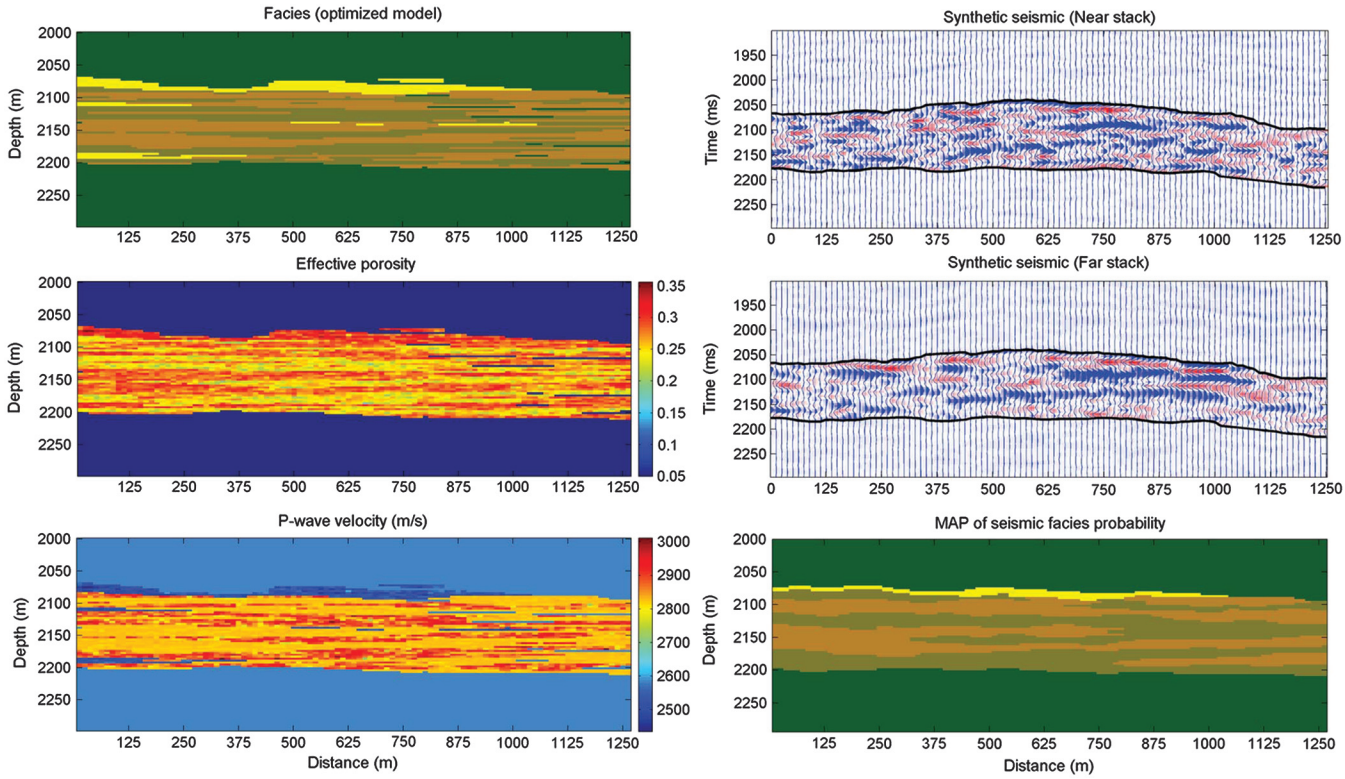


Figure 19. Inversion results along the 2D section shown in Figure 18. On the left, we show the optimized model of reservoir facies (top left), porosity (mid left), and P-wave velocity (bottom left) obtained by stochastic inversion. On the right, we show the corresponding synthetic seismic sections, near (top right) and far (top left) and the maximum a posteriori (MAP) of seismic facies probability (converted in depth and mapped in the geocellular grid) used as secondary information in the Tau model and obtained by multistep inversion (shale in green, silty-sand in brown, stiff sand in light brown, and soft sand in yellow).

single scattering approximation of the first order. However, other techniques could be used such as the reflectivity methods (Kennett algorithm) or 2D Born filtering. Similarly, different rock-physics models could be introduced to link elastic and petrophysical properties.

A limitation of this methodology is the presence of tuneable parameters, such as the Tau model exponents, variogram parameters, and the optimization tolerance. The determination of the Tau-model weights is still a subject of research, and a methodology to quantitatively express the data-dependency or the dependency of the probabilistic information, through the Tau-model exponents, is still missing. Especially when redundant information is incorporated in the Tau-model, it is recommended to perform a preliminary sensitivity analysis on the parameters of the Tau model, possibly at the well location where a facies classification is generally provided by formation evaluation studies. In our study, we used $\tau_1 = \tau_2 = 1$ and $\tau_3 = 0.5$ after some synthetic tests performed at the well location to investigate the effect of the Tau model parameters, but the final choice is partially a subjective decision. The optimization tolerance $T$ significantly influences the variability of the set of models of multiple realizations; the smaller the tolerance, the smaller the variability within the set of models obtained from different runs. This choice is related to how well we want to match the data. This parameter depends on several conditions related to the seismic data set of the reservoir study and it should be assessed by trial and error. A similar conclusion can be drawn for variogram parameters. In this case, an assessment of the parameters is harder, especially for the correlation ranges in the lateral directions, due to the lack of multiple wells distributed spatially. We have seen that, in the 1D application, the key is to select the appropriate parameters to reconcile the expected vertical variogram and the match with real seismic data, but this assessment cannot be done in a 2D or 3D application unless a very large number of wells are available. The assumptions related to the choice of correlation ranges and anisotropic parameters of the variogram model are crucial; in real reservoir studies, this choice only can rely on prior geologic information of the field or nearby fields. We observed that solutions are better, with finer scale features, when the variogram range is underestimated. As pointed out by an anonymous reviewer, this behavior may be quite general. By giving a short range, we specify a prior information outside the seismic bandwidth and the inversion process can adapt better the solution to the specified prior (i.e., it has more freedom to arrange the thin layers in a way that gives a good seismic response). On the contrary, if we specified a long range, the prior may be less complementary to the seismic frequency content. In the case of a wrong prior (too-large thickness linked to an overestimation of the ranges), it may be then more difficult for the inversion algorithm to adapt the (thick) layers to give the assigned seismic response. Seismic data could be used to estimate these properties, but the lateral continuity of seismic is generally affected by the migration operator applied to data, which could lead to an overestimation of the lateral ranges of the variograms.

One possible future development is to use a multiparameter approach in the probability perturbation method (MP-PPM), where we optimize more than one parameter simultaneously. One particular property that could be made stochastic and perturbed in this manner is the facies proportion, especially when few wells are available in the field.

## CONCLUSION

We presented a new methodology for facies and reservoir properties modeling that combines traditional geophysical models, such as rock-physics and seismic forward modeling, with geostatistical methods. The proposed approach is a stochastic optimization based on the probability perturbation method and Tau model. The use of sequential simulations allows us to generate fine-scaled models, while the probability perturbation method guarantees that the optimized model matches the real data within a fixed tolerance. The main advantage of this technique is that it provides high-resolution models of facies and the associated properties in a moderate amount of computational time. The method is fast, especially if secondary information is provided. This secondary information can be obtained from seismic attributes through different techniques; if the secondary information is not taken into account, the convergence could be quite slow, especially in complex sequences of thin layers, and the assumption of stationarity of geostatistical methods cannot be satisfactorily overcome. Different probabilistic information from different sources and at different scales can be integrated into the methodology thanks to the use of the Tau model.

The application to the real well data shows that the methodology can be applied to complex reservoirs with good results.

## ACKNOWLEDGMENTS

We acknowledge Stanford Rock Physics and Borehole Geophysics Project (SRB), and Stanford Center for Reservoir Forecasting (SCRF) for the support. We also acknowledge the reviewers for the helpful comments and suggestions.

## APPENDIX A

## TWO-POINT GEOSTATISTICS

SGSim is a geostatistical method that allows us to generate several realizations of a continuous property which honor: (1) the hard data (if any) used to condition the simulation, (2) the target distribution (if the distribution of the property is not already a standard Gaussian PDF), and (3) the variogram model which describes the spatial continuity of the property. In SGSim, we sequentially visit the grid cells along a random path. At each cell, we simulate a value by sampling from a Gaussian distribution with mean equal to the kriging estimate at that location and variance equal to the kriging variance. Kriging estimate and variance at the given location are computed by solving the kriging system (Goovaerts, 1997). The procedure is repeated for all the cells in the grid. As in many practical applications, when the target distribution is not Gaussian, we usually apply a preliminary normal score transformation, perform the simulation, and back-transform the results at the end. Sequential Gaussian simulation provides a higher detailed map of the simulated property compared to the corresponding smoothed kriging map. Multiple simulations are generated by changing the random seed.

Sequential indicator simulation can be seen as a generalization of SGSim. It is based on the concept of indicator variable, i.e., a binary variable, which is the indicator of occurrence of an event. SISim is generally applied to simulate discrete properties. The probability of a certain cell assuming a certain value of a discrete property, given the set of neighboring values, is calculated by indicator kriging. In indicator kriging, we estimate the probability of a certain categorical event at a given location as a weighted linear combination of the

indicator data falling within the searching neighborhood. As in traditional kriging, the weights are obtained by solving the linear system of kriging equations, which accounts for the indicator spatial covariance model (Goovaerts, 1997). The methodology relies on the result that the expected value of a binary indicator is the probability of the corresponding categorical event occurring; kriging, as a least-square error estimation method, allows calculating this probability. At each generic location $x_n$ of the random path, we compute the indicator kriging probability $P^{IK}_{f_k}$ of the generic categorical event $f_k$:

$$P^{IK}_{f_k}(x_n) = \pi_{f_k} + \sum_{i=1}^{n-1} w_i(i(x_i, f_k) - \pi_{f_k}), \qquad \text{(A-1)}$$

where $\pi_{f_k}$ is the prior probability of the categorical event $f_k$, $\{i(x_i, f_k)\}_{i=1,\ldots,n-1}$ are the indicators of the previously simulated values at the locations $x_i$, and $w_i$ are the kriging weights. By computing this distribution at each location and sampling from it, SISim allows us to perform simulations of discrete variables such as facies or lithofluid classes.

## APPENDIX B

## PROBABILITY OF SEISMIC FACIES

We describe here the mathematical details of the multistep inversion approach used to estimate the probability of facies at seismic scale. For the complete mathematical description, we refer to Grana and Della Rossa (2010). This method is a full Bayesian approach and it allows us to propagate uncertainty from seismic to facies domain by including various sources of uncertainty: seismic inversion, scale changes, model approximations, heterogeneity, and natural variability of the rocks in the subsurface. In the following, we will use $\mathbf{R}$ for petrophysical properties (porosity, clay content, and possibly, water saturation), $\mathbf{m}$ for elastic properties (impedances) at fine scale, and $\mathbf{S}$ for elastic properties at coarse (seismic) scale (seismic impedances, AVO attributes, or seismic amplitudes).

By means of statistical rock-physics models, we can estimate the probability of petrophysical properties conditioned by elastic properties $P(\mathbf{R}|\mathbf{m})$ and the probability of elastic properties given the seismically derived attributes $P(\mathbf{m}|\mathbf{S})$. By combining these probabilities, we obtain the posterior distribution of petrophysical properties by means of the following equation (Grana and Della Rossa 2010):

$$P(\mathbf{R}|\mathbf{S}) = \int_{R^n} P(\mathbf{R}|\mathbf{m})P(\mathbf{m}|\mathbf{S})d\mathbf{m}. \qquad \text{(B-1)}$$

The likelihood function in the statistical rock-physics model is based on the assumption of Gaussian mixture distribution of petrophysical properties, which is a reasonable assumption whenever petrophysical attributes describe different facies features. If this is the case, the weights of the mixture $\lambda_k(\mathbf{m})$ can be interpreted as the conditional probability of facies occurrence. Mathematically, the rock-physics likelihood function can be expressed as

$$P(\mathbf{R}|\mathbf{m}) = \sum_{k=1}^{N_F} \lambda_k(\mathbf{m})N(\mathbf{R}; \boldsymbol{\mu}^k_{\mathbf{R}|\mathbf{m}}, \boldsymbol{\Sigma}^k_{\mathbf{R}|\mathbf{m}}), \qquad \text{(B-2)}$$

where $N_F$ is the number of facies, and $\boldsymbol{\mu}^k_{\mathbf{R}|\mathbf{m}}$ and $\boldsymbol{\Sigma}^k_{\mathbf{R}|\mathbf{m}}$ are the conditional means and the covariance matrices of the Gaussian mixture components, respectively.

The methodology is then extended to the discrete domain to estimate facies probabilities based on seismic data or seismically derived attributes. The posterior probability of lithofacies is computed as

$$P^*(\mathbf{F}|\mathbf{S}) = \int_{R^m} P(\mathbf{F}|\mathbf{R})P(\mathbf{R}|\mathbf{S})d\mathbf{R} = \int\int_{R^{m+n}} P(\mathbf{F}|\mathbf{R})P(\mathbf{R}|\mathbf{m})P(\mathbf{m}|\mathbf{S})d\mathbf{R}d\mathbf{m}, \qquad \text{(B-3)}$$

where the probability $P(\mathbf{R}|\mathbf{S})$ is obtained by means of equation B-1 and the rock-physics likelihood $P(\mathbf{F}|\mathbf{R})$ is assumed to be independent of seismic and is calibrated using well logs: petrophysical curves and log facies classification. The final results of this method are the probability volumes $P^*(\mathbf{F}|\mathbf{S})$ of seismic lithofacies. In the stochastic inversion, the probability $P^*(\mathbf{F}|\mathbf{S})$ is integrated as an additional information in the Tau model.

## REFERENCES


Aki, K., and P. G. Richards, 1980, Quantitative seismology: W. H. Freeman & Co..

Avseth, P., T. Mukerji, A. Jørstad, G. Mavko, and T. Veggeland, 2001, Seismic reservoir mapping from 3-D AVO in a North Sea turbidite system: Geophysics, **66**, 1157–1176, doi: 10.1190/1.1487063.

Avseth, P., T. Mukerji, and G. Mavko, 2005, Quantitative seismic interpretation: Cambridge University Press.

Bosch, M., C. Carvajal, J. Rodrigues, A. Torres, M. Aldana, and J. Sierra, 2009, Petrophysical seismic inversion conditioned to well-log data: Methods and application to a gas reservoir: Geophysics, **74**, no. 2, O1–O15, doi: 10.1190/1.3043796.

Bosch, M., T. Mukerji, and E. F. Gonzalez, 2010, Seismic inversion for reservoir properties combining statistical rock physics and geostatistics: A review: Geophysics, **75**, no. 5, 75A165–75A176, doi: 10.1190/1.3478209.

Buland, A., O. Kolbjørnsen, R. Hauge, O. Skjæveland, and K. Duffaut, 2008, Bayesian lithology and fluid prediction from seismic prestack data: Geophysics, **73**, no. 3, C13–C21, doi: 10.1190/1.2842150.

Buland, A., and H. Omre, 2003, Bayesian linearized AVO inversion: Geophysics, **68**, 185–198, doi: 10.1190/1.1543206.

Caers, J., and T. B. Hoffman, 2006, The probability perturbation method: A new look at Bayesian inverse modeling: Mathematical Geology, **38**, no. 1, 81–100, doi: 10.1007/s11004-005-9005-9.

Castro, S. A., J. Caers, C. Otterlei, H. Meisingset, T. Hoye, P. Gomel, and E. Zachariassen, 2009, Incorporating 4D seismic data into reservoir models while honoring production and geologic data: A case: The Leading Edge, **28**, 1498, doi: 10.1190/1.3272706.

Deutsch, C., and A. G. Journel, 1992, GSLIB: Geostatistical software library and user's guide: Oxford University Press.

Doyen, P., 2007, Seismic reservoir characterization: EAGE.

Eidsvik, J., P. Avseth, H. Omre, T. Mukerji, and G. Mavko, 2004, Stochastic reservoir characterization using prestack seismic data: Geophysics, **69**, 978–993, doi: 10.1190/1.1778241.

González, E. F., T. Mukerji, and G. Mavko, 2008, Seismic inversion combining rock physics and multiple-point geostatistics: Geophysics, **73**, no. 1, R11–R21, doi: 10.1190/1.2803748.

Goovaerts, P., 1997, Geostatistics for natural resources evaluation: Oxford University Press.

Grana, D., and E. Della Rossa, 2010, Probabilistic petrophysical-properties estimation integrating statistical rock physics with seismic inversion: Geophysics, **75**, no. 3, O21–O37, doi: 10.1190/1.3386676.

Grana, D., E. Della Rossa, and C. D'Agosto, 2009, Petrophysical properties estimation in a crosswell study integrated with statistical rock physics: 79th Annual International Meeting, SEG, Expanded Abstracts, 1805–1809.

Gunning, J., and M. Glinsky, 2007, Detection of reservoir quality using Bayesian seismic inversion: Geophysics, **72**, no. 3, R37–R49, doi: 10.1190/1.2713043.

Hansen, T. M., K. S. Cordua, and K. Mosegaard, 2012, Inverse problems with non-trivial priors: Efficient Solution through sequential Gibbs

sampling: Computational Geosciences, 1–19, doi: 10.1007/s10596-011-9271-1.
Journel, A. G., 2002, Combining knowledge from diverse sources: An alternative to traditional conditional independence hypothesis: Mathematical Geology, **34**, no. 5, 573–596, doi: 10.1023/A:1016047012594.
Journel, A. G., and J. J. Gomez-Hernandez, 1989, Stochastic imaging of the Wilmington clastic sequence: SPE Formation Evaluation, **8**, no. 1, 33–40, doi: 10.2118/19857-PA, SPE 19857-PA.
Krishnan, S., 2008, The Tau model for data redundancy and information combination in earth sciences: Theory and application: Mathematical Geology, **40**, no. 6, 705–727, doi: 10.1007/s11004-008-9165-5.
Krumbein, W. C., and M. F. Dacey, 1969, Markov chains and embedded Markov chains in geology: Mathematical Geology, **1**, no. 1, 79–96, doi: 10.1007/BF02047072.
Larsen, A. L., M. Ulvmoen, H. Omre, and A. Buland, 2006, Bayesian lithology/fluid prediction and simulation on the basis of a Markov-chain prior model: Geophysics, **71**, no. 5, R69–R78, doi: 10.1190/1.2245469.
Liu, Y., 2003, Downscaling seismic data into a geologically sound numerical model: Ph.D. thesis, Stanford University.
Mavko, G., T. Mukerji, and J. Dvorkin, 2009, The rock physics handbook: Cambridge University Press.
Mukerji, T., A. Jørstad, P. Avseth, G. Mavko, and J. R. Granli, 2001, Mapping litho-facies and pore-fluid probabilities in a North Sea reservoir: Seismic inversions and statistical rock physics: Geophysics, **66**, 988–1001, doi: 10.1190/1.1487078.
Remy, N., A. Boucher, and J. Wu, 2009, Applied geostatistics with SGeMS: Cambridge University Press.
Rimstad, K., and H. Omre, 2010, Impact of rock-physics depth trends and Markov random fields on hierarchical Bayesian lithology/fluid prediction: Geophysics, **75**, no. 4, R93–R108, doi: 10.1190/1.3463475.
Stright, L., A. Bernhardt, A. Boucher, T. Mukerji, and R. Derksen, 2009, Revisiting the use of seismic attributes as soft data for subseismic facies prediction: Proportion versus probabilities: The Leading Edge, **28**, 1460–1469, doi: 10.1190/1.3272701.
Tarantola, A., 2005, Inverse problem theory: SIAM.
Ulvmoen, M., and H. Omre, 2010, Improved resolution in Bayesian lithology/fluid inversion from prestack seismic data and well observations: Part 1 — Methodology: Geophysics, **75**, no. 2, R21–R35, doi: 10.1190/1.3294570.
Wilschut, F., E. Peters, K. Visser, P. A. Fokker, and P. M. E. van Hooff, 2011, Joint history matching of well data and surface subsidence observations using the ensemble Kalman filter: A field study: SPE Reservoir Simulation Symposium, 141690-MS.